NONLINEAR RESONANT PHOTOIONIZATION IN
MOLECULAR IODINE

by

GEORGENA SARAH PETTY SIL

B.Sc., University of Saskatchewan, 1973

A THESIS SUBMITTED IN PARTIAL FULFILLMENT OF
THE REQUIREMENTS FOR THE DEGREE OF
MASTER OF SCIENCE

in

THE FACULTY OF GRADUATE STUDIES
Department of Physics

We accept this thesis as conforming
to the required standard

THE UNIVERSITY OF BRITISH COLUMBIA
September, 1976

In presenting this thesis in partial fulfillment of the requirements for an advanced degree at the University of British Columbia, I agree that the Library shall make it freely available for reference and study. I further agree that permission for extensive copying of this thesis for scholarly purposes may be granted by the Head of my Department or by his representatives. It is understood that copying or publication of this thesis for financial gain shall not be allowed without my written permission.

Department of Physics

The University of British Columbia
2075 Wesbrook Place
Vancouver, Canada
V6T 1W5

Date *September 25, 1976*

ABSTRACT

Strong photoionization spectra have been observed in molecular Iodine following laser excitation in the near ultraviolet. The dependence upon laser power, and the structure of the spectra are consistent with three-photon ionization with resonance in an intermediate state excited by two photons. Vibrational analysis indicates an electronic energy T_e of 53,562.75 ± 1 cm^{-1}, a harmonic vibrational constant ω_e of 241.4 ± 0.4 cm^{-1}, and an anharmonic vibrational constant $\omega_e x_e$ of 0.58 ± 0.06 cm^{-1}. Rotational analysis done by the Franck-Condon method, whereby the relative experimental band intensities are compared with theoretical values, indicates that the internuclear separation r_e in the resonant electronic state is 2.567 ± 0.002Å, corresponding to a rotational constant B_e of 0.04029 ± 0.00007 cm^{-1}. The new electronic state has, with high probability, the designation 1_g. Several impurity lines were observed at exciting energies 26,297.14 ± 1 cm^{-1} (half width 8.09 cm^{-1}), at 26,915.22 ± 1 cm^{-1}, and at 27,343.96 ± 1 cm^{-1}. The impurity signal varies as $I_0^{2.02}$. The features likely arise from complex molecular species formed in reactions at high temperature with I_2, and have not been identified. The photoionization efficiency of I_2 in nonlinear absorption exhibits an apparent resonance in the vicinity of 80,000 cm^{-1} in terms of total molecular energy.

TABLE   OF   CONTENTS

TABLE OF CONTENTS (cont.)

LIST OF TABLES

LIST OF TABLES (cont.)

LIST OF FIGURES AND ILLUSTRATIONS

FIGURES AND ILLUSTRATIONS (cont.)

ACKNOWLEDGEMENT

To my Father

1. INTRODUCTION

A number of nonlinear phenomena have been investigated since the introduction of the laser as a spectroscopic tool. All of the earliest work was done in solids in which the generation of second-order optical harmonics and parametric conversion was achieved, among others, by Franken et al. (1961) and Giordmaine (1962). The intensity of the generated nonlinear component is limited by interference due to the normal dispersion of the material. It was soon discovered that the only means of enhancing the nonlinear output to practical magnitudes was to employ strongly birefringent crystals in which, upon rotation, matching of the refractive indices of the incident and generated waves is possible (Baldwin, 1969 and Zernike, 1973). The inert gases and atomic and molecular vapors became materials of interest somewhat later. In a few cases (Miles and Harris, 1973 and Young et al., 1973) enhancement techniques were pursued similar to those in solids, in which phase-matching was achieved through precise mixing of gases. Most of the work, however, involved enhancement of the nonlinear response through at least one resonance with an atomic or molecular state, made practical with the development of tunable, narrow-bandwidth lasers circa 1970. This resonant-enhancement technique is becoming not only a means of parametric conversion and generation of coherent far-ultraviolet radiation in gases

and vapors, but also a means of gaining spectroscopic informa-
tion about atoms and molecules heretofore inaccessible. Very
little work has been carried out to date in this field. Among
other experiments, DC-induced second harmonic generation in
the inert gases was observed by Finn and Ward (1971), and
third-order optical components were generated in atomic vapors
by Hodgson et al. (1974) and Leung et al. (1974). Resonance
fluorescence in molecular Iodine following two-photon excita-
tion of the low-lying E state has been studied by Rousseau
and Williams (1974).

The particular nonlinear interaction which is the
subject of the present work is multiphoton absorption and
ionization of molecules under the influence of tunable laser
radiation. As with most nonlinear phenomena in gases and
vapors, multiphoton ionization has received renewed interest
only during the last four years or so. Theoretical investi-
gations have been carried out by Lambropoulos (1974) and
Pindzola and Kelly (1975), and experimental work has been
done by Bakos et al. (1972), Collins et al. (1973), Collins
et al. (1974), Delone et al. (1972), LuVan and Mainfray (1972),
and LuVan et al. (1972) upon the elements He, K, Na, Cs,
Cs_2, N_2 and H_2. The multiphoton ionization process is
described as follows. When a molecule is ionized in a strong
electromagnetic field of optical frequency, a situation may
arise wherein the energy of several quanta turns out to be

equal to the energy of the bound state of the electrons.
In this case the ionization will proceed in two stages,
multiphoton resonant excitation of the molecule and ioniza-
tion of the excited molecule. The second stage can also
have the character of a multiphoton transition (Delone et al.,
1972). When ionization occurs via an intermediate resonant
state, new and significant spectroscopic information may be
obtained regarding the electronic structure and spectroscopic
parameters of molecular states which are inaccessible, for
a variety of reasons, using conventional absorption spectro-
scopy. Transitions which are parity-forbidden in one-step
processes may be investigated in multiphoton spectroscopy
if the resonant excited state lies at an energy above the
ground state corresponding to an even number of quanta of
incident energy. Multiphoton spectroscopy has the additional
advantage of allowing detailed investigation of high-energy
electronic states using visible light sources. In the past,
population of both parity-forbidden and high-energy states
could be accomplished only by high-energy excitation (for
example, electrical discharges) in which many other electronic
states were simultaneously excited. The subsequent re-emission
was generally extremely complicated and the assignments were
at best ambiguous. In contrast, multiphoton experiments
can selectively populate such forbidden states without inter-
ference from other electronic states. Multiphoton spectroscopy

also has the advantage also has the advantage of reducing Doppler broadening in applications such as double-beam experiments (Bloembergen, 1965 and Cagnac et al., 1973).

Molecular Iodine is the subject of the present multi-photon investigations. The nature and identification of the higher valence-shell states and the Rydberg states of I_2 remain confused and controversial, and even some aspects of the lower valence-shell states are in controversy. Molecular Iodine has been extensively studied both in absorption and in emission, and a great many papers have been devoted to the correlation of experimental evidence with predictions on the potential curves and other features of the numerous electronic states. Nevertheless, a number of contradictory statements regarding this molecule exist even in the more recent literature. The analyses of Haranath and Rao (1958), LeRoy (1970a and 1970b), Mathieson and Rees (1956), Mulliken (1971), Nobs and Wieland (1966), and Venkateswarlu (1970) conflict on the points:

(a) the number of band systems in certain regions of the spectrum, and the arrangement of bands into these systems,

(b) the final states in the ultraviolet resonance fluorescence systems,

(c) the basic spectroscopic constants (vibrational and rotational frequencies, electronic potential-well

minima, and dissociation energies) of both high-
and low-energy states,

(d) electronic configurations and dissociation products
of the upper states.

This amply demonstrates that I_2 with its very complex spec-
trum is a good candidate for investigation by multiphoton
techniques.

In the present work, the Iodine molecule is excited in
the near ultraviolet with a pulsed, continuously tunable,
narrow-bandwidth laser. It is known that the spectrum of
Iodine changes in the presence of foreign gases such as argon
and nitrogen, and thus the experimental work was performed
in pure Iodine vapor which was distilled into an evacuated
cell. The experimental conditions are such that we expect
triple-photon ionization of the Iodine molecule via the
reaction:

$$I_2 + 3\nu \rightarrow I_2^+ + e^- ,$$
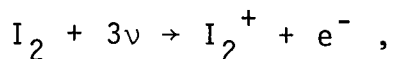
accompanied by a very small percentage of triple-photon dis-
sociation. As discussed in Chapter 2, any resonances which
occurs in I_2 will correspond to an intermediate state excited
by two photons. The range of exciting energy is 26,316 -
27,397 cm^{-1}. Thus the accessible resonant transitions are
those which are parity-forbidden from the ground electronic
state and whose energy lies between 52,632 and 54,794 cm^{-1}.
In what follows, vibrational and rotational analysis is

carried out, and the assignment of the electronic configuration is attempted, upon a new electronic state observed in I_2 via resonant enhancement of the nonlinear photoelectron signal. This research contributes to the spectroscopic information of the Iodine molecule, but more important, this research contributes to the development of a new spectroscopic tool which, in view of its sensitivity and simplicity, is expected to have significant applications.

2. THEORY AND ANALYTIC TECHNIQUES

2.1 Theory of Nonlinear Optics

The dielectric constant ε in Maxwell's constituitive relation $\vec{D} = \varepsilon\vec{E}$ is in general a function of the field strength $|\vec{E}|$. The nonlinear terms are very small at optical frequencies, however, and thus their experimental discovery occurred only after the development of powerful lasers. For pure electric dipole interactions, which form the strongest optical transitions in molecules, we may expand the polarization $\vec{P}$ in a power series in the applied electric field $\vec{E}$ as follows:

$$\vec{P} = \varepsilon_0 \, \chi \, \vec{E}\left(1 + \frac{\vec{E}}{a_1} + \left(\frac{\vec{E}}{a_2}\right)^2 + \left(\frac{\vec{E}}{a_3}\right)^3 + \cdots \right) . \qquad (2.1)$$

For any atom or molecule, the parameters a_1, a_2, a_3, etc. are on the order of the magnitude of the electric field E_m inside the atom or molecule, typically about 3×10^8 volts/cm (Bloembergen, 1965). Thus we may write

$$\vec{P} \simeq \varepsilon_0 \, \chi \, \vec{E} \left(1 + \frac{\vec{E}}{E_m} + \left(\frac{\vec{E}}{E_m}\right)^2 + \left(\frac{\vec{E}}{E_m}\right)^3 + \cdots \right) .$$

Since the ratio $|\vec{E}|/E_m \leq 3 \times 10^{-3}$ in the focus of the most powerful lasers available (Bloembergen, 1965), the nonlinear response is very small.

Each order of nonlinearity requires its own expression for the susceptibility χ, and thus χ must take the form of

a tensor when describing nonlinear phenomena. The general expression for a susceptibility coefficient of Nth order in the standard notation of the literature is $\chi(-\omega^o; \omega_1, \omega_2, \ldots, \omega_N)$ where the frequencies ω_i of the applied electric fields satisfy $\omega^o = \omega_1 + \omega_2 + \cdots + \omega_N$. Since in this research only one light source is used, all ω_i are equal and hence $\omega^o = N\omega$. Thus, the expressions for the susceptibility coefficients for polarizations linear, second order, and third order in the applied electric field $\vec{E}(\omega)$ may be written (Guccione-Gush et al., 1967, Lambropoulos, 1974, Leung et al., 1974):

LINEAR

$$\chi(-\omega; \omega) \propto \frac{-\langle \psi_g^o | \vec{M} | \psi_n^o \rangle}{(\Omega_{ng} - \omega)}$$

SECOND ORDER

$$\chi(-2\omega; \omega, \omega) \propto \sum_{\ell} \frac{\langle \psi_g^o | \vec{M} | \psi_\ell^o \rangle \langle \psi_\ell^o | \vec{M} | \psi_n^o \rangle}{(\Omega_{\ell g} - \omega)(\Omega_{ng} - 2\omega)}$$

THIRD ORDER

$$\chi(-3\omega; \omega, \omega, \omega) \propto \sum_{\ell, m} \frac{\langle \psi_g^o | \vec{M} | \psi_\ell^o \rangle \langle \psi_\ell^o | \vec{M} | \psi_m^o \rangle \langle \psi_m^o | \vec{M} | \psi_n^o \rangle}{(\Omega_{\ell g} - \omega)(\Omega_{mg} - 2\omega)(\Omega_{ng} - 3\omega)}$$

$\vec{M}$ is the electric dipole-moment operator of section 2.4. The state $|\psi_g^o\rangle$ is the ground state of the system, and $|\psi_\ell^o\rangle$, $|\psi_m^o\rangle$, $|\psi_n^o\rangle$ are eigenstates of succeedingly higher energies, $|\psi_n^o\rangle$ being the final state in absorption precesses. When absorption leads to ionization, the matric element

$\langle \psi_n^0 | \vec{M} | \psi_g^0 \rangle$ between the final and initial states need not be included in the susceptibilities. An upper state, for example $| \psi_\ell^0 \rangle$, has energy $\hbar c \omega_\ell$ and lifetime Γ_ℓ^{-1}, and $\Omega_{\ell g}$ defined by:

$$\Omega_{\ell g} = (\omega_\ell - \omega_g) - (i/2) \Gamma_\ell \quad .$$

The form of the susceptibility coefficients indicates that the nonlinear polarizability may be enhanced whenever a resonance in one of the factors in the denominator of the susceptibility occurs. Such a resonance occurs whenever the applied field frequency ω is such that the real part of a resonance factor in the denominator vanishes. For third-order nonlinearities, for example, which is the subject of this research, we require for resonance enhancement at least one of the following:

$$R_e(\Omega_{\ell g} - \omega) = 0, \quad \text{or}$$
$$R_e(\Omega_{mg} - 2\omega) = 0, \quad \text{or}$$
$$R_e(\Omega_{ng} - 3\omega) = 0.$$

These relationships are equivalent to:

$$\omega_\ell - \omega_g = \omega \ , \quad \text{or}$$
$$\omega_m - \omega_g = 2\omega, \quad \text{or}$$
$$\omega_n - \omega_g = 3\omega \quad .$$

_____ n

_____ m

_____ ℓ

_____ ground
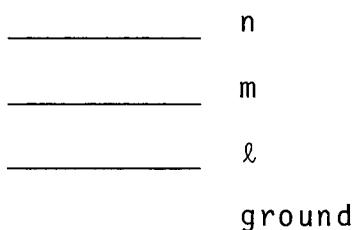
EIGENSTATES OF THE SYSTEM

As well, the appropriate matrix elements must not vanish (see section 2.4).

In order that the incident light energy not be lost through scattering or linear absorption, we must tune <u>away</u> from resonance with regards to the first excited state. Thus the state $|\psi_\ell^0\rangle$ is a virtual state and $|(\omega_\ell - \omega_g) - \omega| \gg 0$. On the other hand, both of the uppermost states $|\psi_m^0\rangle$ and $|\psi_n^0\rangle$ may be resonant, or real states. However, since the final state $|\psi_n^0\rangle$ is a continuum state in the photoionization process, no significant spectroscopic information would be gained if this were the only resonant state. Thus, we focus on the discrete second excited state $|\psi_m^0\rangle$ as the necessary resonant state, resonant enhancement occurring when twice the energy of the fundamental photon becomes equal to the energy difference between $|\psi_m^0\rangle$ and the ground state of the molecule:

$$\omega_m - \omega_g = 2\omega \quad .$$

Two-photon resonance has the advantage of allowing detailed investigation of electronic states which are symmetry-

forbidden in linear (one-photon) spectroscopy, as shown in section 2.4. The order of the states is then, for two-photon resonant, triple-photon ionization of the Iodine molecule:

n _____ continuum ($\geq$ 75,814 $\pm$ 10 cm^{-1})

m _____ resonant

ℓ _____ virtual

g _____ XO_g^+ ground

The use of a tunable dye laser as the source of the applied electric field provides an absorption spectrum as a continuous function of wavelength over the useful range of the laser dye, and hence as a function of the identity of the resonant states $|\psi_m^o\rangle$.

When N photons are involved in the transition, the photoionization signal intensity S depends upon the Nth power of the intensity I_o of the incident light. This follows from equation 2.1 in which the nonlinear polarizability in Nth order depends upon the Nth power of the electric field vector. Thus if C is a proportionality constant we may write:

$$S = C\, I_o^{\,N} \quad .$$

The signal is expected to vary as $I_o^{\,3}$. The power-dependence of our photoionization signal may be measured experimentally in the following manner. When a number n of calibrated neutral

density filters, each of the same density $K(\lambda)$, are used to
attenuate the laser beam before it enters the Iodine chamber,
then the photoionization signal S is attenuated as follows:

$$S = C \, I_0{}^N \, 10^{-K(\lambda)nN} \; ,$$

or, in a more convenient form:

$$\log S = \log(C \, I_0{}^N) - K(\lambda)nN$$
$$= \text{constants} - K(\lambda)nN \quad .$$

The power dependence N may be determined from the slope of a
plot of the log of the photoionization signal intensity versus
the number of filters in the path of the incident beam, if
the density $K(\lambda)$ is known. We have:

$$N = - \frac{\text{slope}}{K(\lambda)} \; . \tag{2.2}$$

2.2 Coarse Structure: Vibrational Analysis

2.2.1 The anharmonic oscillator

The simple harmonic oscillator model provides only a
first-order approximation to any physical oscillator, since
perfectly elastic forces, which are linearly proportional to
the amplitude of vibration, do not exist in nature. In
particular, the attractive force between any two atoms of a
molecule tends to zero, rather than increasing indefinitely,
with increasing distance from the equilibrium position. The
actual binding force must be represented by power series in

powers of the displacement from equilibrium, and asymmetry requires both even and odd terms. The one-dimensional binding force of a diatomic molecule, in the absence of externally applied fields, is thus:

$$F = \text{Harmonic Term} + \text{Anharmonic Terms}$$
$$= -k_1(r - r_e) + k_2(r - r_e)^2 - k_3(r - r_e)^3 + \cdots$$

where r is the internuclear separation, r_e is the equilibrium separation, and k_1, k_2, k_3 are force constants. The corresponding potential energy function, which is electronic in nature, in which the nucleii move is:

$$U = k_1/2(r - r_e)^2 - k_2/3(r - r_e)^3 + k_3/4(r - r_e)^4 + \cdots$$

For small anharmonicity of the oscillator ($|k_3| << |k_2| << |k_1|$) the eigen energies of the Schroedinger equation may be determined with a perturbation calculation to be:

$$E_v = hc\omega_e(v + \tfrac{1}{2}) - hc\omega_e x_e(v + \tfrac{1}{2})^2 + hc\omega_e y_e(v + \tfrac{1}{2})^3 + \cdots$$

where h is Planck's constant, c is the velocity of light, v is the vibrational quantum number, and ω_e, $\omega_e x_e$, $\omega_e y_e$, $\cdots$ are constants characterizing the molecule, proportional to the force constants. The quantities $\omega_e x_e$, $\omega_e y_e$, $\cdots$ are a measure of the anharmonicity of the molecule, while ω_e is the harmonic approximation to the oscillator frequency ($\omega_e = \sqrt{k_1/\mu}$, where μ is the reduced mass). A more useful

expression in spectroscopy is the "vibrational term" G(v) in wavenumber units given by

$$G(v) = \omega_e(v + \tfrac{1}{2}) - \omega_e x_e(v + \tfrac{1}{2})^2 + \omega_e y_e(v + \tfrac{1}{2})^3 + \cdots$$

$$(2.3)$$

for the anharmonic oscillator. Although the vibrational motion is still strictly periodic, the natural or resonant frequency is amplitude-dependent, the frequency decreasing with increasing amplitude. Furthermore, due to the asymmetry of the potential curve, the time average of the position of the oscillator is no longer the equilibrium position, but, for almost all molecules, is greater ($\langle r \rangle > r_e$).

The separation of successive vibrational levels is described in wavenumber units by the following

FIRST DIFFERENCE

$$\Delta G_{v,v+1} \equiv G(v+1) - G(v)$$
$$= \omega_e - \omega_e x_e(2v+2) + \omega_e y_e(3v^2+6v+13/4) + \cdots$$

$$(2.4)$$

SECOND DIFFERENCE

$$\Delta^2 G_{v,v+2} \equiv \Delta G_{v,v+1} - \Delta G_{v+1,v+2}$$
$$= 2\,\omega_e x_e - \omega_e y_e(6v+9) + \cdots$$

$$(2.5)$$

where v is by definition the quantum number of the lowest vibrational state involved in the comparison. While $\omega_e y_e$ may be positive or negative, $\omega_e x_e$ is positive for nearly all

diatomic molecules (Herzberg, 1950). Thus the vibrational levels draw together with increasing vibrational quantum number, and eventually merge into a continuum.

In this work, the standard spectroscopic notation is adopted whereby v' represents the upper, and v" the lower state involved in a vibrational transition. A series of transitions which involves a single upper state and several adjacent lower states (or vice versa) is termed a progression. See section 2.4 for a discussion of vibrational selection rules.

2.2.2 Thermal distribution of the vibrational states

According to the Maxwell-Boltzmann distribution law applied to quantum mechanics under conditions of thermal equilibrium, the number of molecules N_v in each of the vibrational states is proportional to the Boltzmann factor $e^{-E/kT}$, where k is the Boltzmann constant, T is the absolute temperature in degrees Kelvin, and E is the energy of vibration (Herzberg, 1950). If E is defined as the vibrational energy measured from the first state,

$$E = G(v) - G(0)$$
$$\equiv G_0(v)$$

then the Boltzmann factor $e^{-G_0(v)/kT}$ gives the relative numbers of molecules in the different vibrational levels referred to the number of molecules in the lowest vibrational

level. When $G_0(v)$ is expressed in wavenumber units, then substitution of the constant k gives the result

$$\frac{N_v}{N_0} = e^{-G_0(v)/(0.6952 \text{ cm}^{-1}/°K)T} \qquad .$$

If we wish to determine N_v relative to the total number N of molecules in the gas sample, the so-called partition function Q_v is required in which the Boltzmann factors are summed over all states:

$$Q_v = \sum_v e^{-G_0(v)/(0.6952 \text{ cm}^{-1}/°K)T} \qquad .$$

Then the fractional number of molecules in vibrational state v is

$$\frac{N_v}{N} = \frac{e^{-G_0(v)/(0.6952 \text{ cm}^{-1}/°K)T}}{Q_v} \qquad .$$

In most diatomic gases, only one progression of a band system normally appears, that with $v'' = 0$. For Iodine, however, the vibrational quanta are small because the molecule is relatively heavy, leading to an appreciable population of the upper vibrational states of the ground electronic state at room temperature (see Table XI). Thus, it is predicted that in addition to the $v'' = 0$ to $v' = 0, 1, 2, ..., n$ absorption progression, the progressions $v'' = 1, 2, 3, 4$ (and possibly higher) to $v' = 0, ..., n$ will appear in our data.

2.3 Fine Structure: Rotational Analysis

The simple rigid rotator model provides a first-order
approximation to the rotational motion of a diatomic mole-
cule. In this model we consider the two atoms of reduced
mass μ to be point-like and fastened at a distance r apart
at the ends of a weightless, rigid rod. The solution of the
appropriate Schroedinger equation is comparatively simple
and yields the eigenenergies of rotation, in wavenumber
units:

$$F(J) = BJ(J + 1) \quad , \qquad B \equiv \frac{\hbar}{4\pi c \mu r^2} \quad .$$

J is the rotational quantum number, and r is the internuclear
separation. The rotational constant B is essentially the
reciprocal moment of inertia of the nucleii. For a more
accurate treatment, we must take into consideration the fact
that rotation and vibration take place simultaneously. During
a vibration period, the internuclear distance and consequently
the moment of inertia and rotational constant B are changing.
Since the period of vibration is very small compared to the
period of rotation, we must use a mean B value in the vibra-
tional state considered:

$$B_v = \frac{\hbar}{4\pi c \mu} \cdot \left\langle \frac{1}{r^2} \right\rangle$$

where $\left\langle 1/r^2 \right\rangle$ is the time average of $1/r^2$ during the vibration
period. B_v is somewhat smaller than the constant B_e evaluated

at the equilibrium separation r_e, since with increasing vibration, because of the anharmonicity, the mean nuclear separation will be greater than r_e. To a first (usually satisfactory) approximation, the rotational constant B_v in the vibrational state v is given by:

$$B_v = B_e - \alpha_e (v + \tfrac{1}{2}) \quad , \qquad \alpha_e << B_e \quad .$$

Consideration of the datomic molecule as a nonrigid rotator also brings in a small correction term for centrifugal force, whereby the internuclear distance, and consequently the moment of inertia, increases with increasing energy of rotation. Therefore the rotational constant B is a function of quantum number J, decreasing with increasing J. Although an exact solution of the nonrigid rotator model requires that the energy be expressed in an infinite power series in powers of J(J + 1), very good accuracy is obtained using only the linear and quadratic terms. The rotational term for the nonrigid rotator becomes:

$$F_v(J) = B_v J(J + 1) - D_v J^2 (J + 1)^2,$$

$$D_v = \frac{4 B_v^3}{\omega^2} \qquad\qquad (2.6)$$

where ω is the vibrational frequency. Typically $D_v < 10^{-4} B_v$.

In the models of the simple rotators, the atoms were treated as point masses. Actually, the mass distribution of the electrons revolving about the two nucleii must be taken

into account. The moment of inertia of these electrons is
much smaller than the moment of the two nucleii about the
center of mass, owing to the much smaller mass of the electron.
In spite of this, the corresponding angular momenta are of
the same order of magnitude since the electrons rotate much
more rapidly. The model of a symmetric top fits the diatomic
molecule (two of the three principal moments of inertia are
equal). For a given electronic state, in the absence of
external torques, the total angular momentum $\vec{J}$ is constant in
magnitude and direction, while the electronic angular momentum
$\vec{\Omega}$ about the figure axis is constant in magnitude but not in
direction. In fact, the figure axis rotates at a constant
angle about $\vec{J}$ with the frequency of the vibrating nonrigid
rotator. The energy levels that result from solution of the
wave equation of the symmetric top (Herzberg, 1950) are:

$$F_v(J) = B_v J(J + 1) - D_v J^2 (J + 1)^2 + (A - B_v)\Omega^2 \ ,$$

$$J \geq \Omega \qquad\qquad (2.7)$$

$$\text{with} \quad A = \frac{\hbar}{4\pi c \ I_{\shortparallel}}$$

where $I_{\shortparallel}$ is the moment of inertia of the electrons about an
axis parallel to the figure axis. For a given electronic
state, Ω is constant and has only a small (integral) value.
Thus the rotational levels of the symmetric top are the same
as those of the simple rotator except for a shift in mag-
nitude $(A - B_v)\Omega^2$ characteristic of the electronic state, and

except that levels with $J < \Omega$ are absent.

Since rotational quanta are much smaller than vibrational quanta, a combined rotation-vibration spectrum gives rise to more or less broad wavelength regions (bands) which usually have at one end a sharp edge (band head). In the expression for the total energy of a transition, $\nu = \nu_e + \nu_v + \nu_r$, the quantity $\nu_0 \equiv \nu_e + \nu_v$ is constant for a given band while ν_r is variable. We may write

$$\nu = \nu_0 + F_{v'}(J') - F_{v''}(J'')$$

for absorption, where ν_0 is called the band origin. Neglecting the small correction term in D_v and noting that $\Omega'' \equiv 0$ for the ground electronic state of I_2 we then have:

$$\nu = \nu_0 + (A' - B_v')\Omega'^2 + B_v'J'(J'+1) - B_v''J''(J''+1)$$

$$\equiv \nu_0 + f(\Omega') + B_v'J'(J'+1) - B_v''J''(J''+1) \ .$$

In two-photon processes, we may expect up to five branches of lines (section 2.4) whose wavenumbers are given by the following formulae (J represents the rotational quantum number of the ground state):

$$\Delta J = + 2$$

$$S(J) = \nu_0 + f(\Omega') + 6B_v' + (5B_v'-B_v'')J + (B_v'-B_v'')J^2 \quad (2.8)$$

$$\Delta J = + 1$$

$$R(J) = \nu_0 + f(\Omega') + 2B_v' + (3B_v'-B_v'')J + (B_v'-B_v'')J^2 \quad (2.9)$$

$$\Delta J = 0$$

$$Q(J) = \nu_0 + f(\Omega') + (B_v' - B_v'')J + (B_v' - B_v'')J^2 \qquad (2.10)$$

$$\Delta J = -1$$

$$P(J) = \nu_0 + f(\Omega') - (B_v' + B_v'')J + (B_v' - B_v'')J^2 \qquad (2.11)$$

$$\Delta J = -2$$

$$O(J) = \nu_0 + f(\Omega') + 2B_v' - (3B_v' + B_v'')J + (B_v' - B_v'')J^2$$
$$(2.12)$$

A band head is formed in a branch if the linear and quadratic terms in J have opposite signs.

Case I. If $B_v' < B_v''$ (but $3B_v' > B_v''$) it is easily seen from equations 2.8 to 2.12 that a head is formed in each of the R and S branches, both heads lying to the high-energy side of ν_0. In addition, the Q branch, if it exists, sometimes forms a head very close to ν_0. All branches of the band are degraded to lower-energy, i.e. to the red.

Case II. When $B_v' > B_v''$, heads are formed in the P and O branches, the heads now lying to the low-energy side of ν_0. The Q branch may also form a head, as in case I. All branches of the band are degraded now toward higher energy, i.e. to the violet.

2.4 Selection Rules for Radiative Absorption

If a system exists in an unperturbed state represented by one member of a complete orthonormal set $\{\psi_n^0(r,t)\}$

of stationary-state wavefunctions, then interaction of this system with an electromagnetic wave $\vec{E}$ creates a perturbation, and consequently a change-of-state to the state $\Psi(r,t)$ which may always be expressed as a "mixture" of the eigenstates:

$$\Psi(r,t) = \sum_n C_n(t) \, \psi_n^{\;0}(r,t) \quad .$$

The probability that the system will make a transition to any new eigenstate, say $\psi_m^{\;0}$, under the influence of the external radiation field is given by $C_m^{\;*}(t)C_m(t)$. Determination of the coefficients $C_m(t)$ involves a calculation of the matrix elements $\langle \psi_m^{\;0} | H_E | \psi_n^{\;0} \rangle$ where $\psi_m^{\;0}$, $\psi_n^{\;0}$ are the final and initial states of the system, and H_E is the Hamiltonian associated with the perturbation $\vec{E}$ (Penner, 1959). In a first approximation, the matrix elements of the interaction of an electromagnetic wave with a diatomic molecule reduce to the interaction of the wave with the (variable) electric dipole moment $\vec{M}$ of the molecule whose components are $M_x = \sum_{k=1}^{N} e_k x_k$ (M_y, M_z similar) where the e_k are the charges on the N particles of coordinates x_k, y_k, z_k. Then for small perturbations, the transition probability per unit time, $P_{n \to m}$, is constant and is given by:

$$P_{n \to m} \equiv \frac{C_m^{\;*}(t)C_m(t)}{t} = \frac{2\pi}{3\hbar^2} \langle \psi_m^{\;0} | \vec{M} | \psi_n^{\;0} \rangle^2 \rho_{\nu_{mn}} \quad . \qquad (2.13)$$

The radiation density $\rho_{\nu_{mn}}$ is strictly a property of the

applied field, while the dipole-moment matrix element
characterizes the molecule.

The previous results rest upon the assumption that
there is no spatial variation in the electric field $\vec{E}$ over
the region of the diatomic molecule in which the distribu-
tion of electric charge is appreciable (that is, where the
electronic wavefunction ψ_n^0 is large). This approximation
is valid in any but exceptional cases since in molecular
spectroscopy we are concerned with ultraviolet, visible
and infrared radiation ($\lambda > 1000\overset{o}{A}$) so the wavelengths are
large compared with molecular dimensions ($\simeq 2\overset{o}{A}$). If the
variation of the electric field over the dimensions of the
molecule is not neglected, there appear in the expression
for the transition probability, matrix elements of the
magnetic dipole, electric quadrupole, and higher moments.
However, the matrix elements of the higher moments are many
powers of ten smaller than the matrix element of the dipole
moment, and hence the corresponding transitions are observ-
able only when the dipole transition is forbidden.

The requirement that the transition probability $P_{n \to m}$
given by equation 2.13 be nonzero for the combining states
leads to certain selection rules based on the evaluation of
the dipole matrix element between the given states. For
many would-be transitions this dipole matrix element
vanishes identically, and the transition is termed forbidden.

For example, a homonuclear diatomic molecule such as I_2 has no permanent electric dipole moment and neither its vibrations nor rotations induce a dipole ($\vec{M} \equiv 0$). Therefore it does not interact with radiation to produce a pure vibrational or rotational spectrum. However, such molecules do exhibit electronic spectra with vibrational and rotational structure (bands), because the instantaneous dipole moment changes during the redistribution of electric charge which accompanies the electronic transition (King, 1964). I_2 conforms to Hund's coupling case c, in which the L-S coupling of the separate atoms persists when the molecule is formed. The component of total angular momentum along the internuclear axis, Ω, is well-defined. For the diatomic molecule I_2, the transitions which are allowed may be categorized under the following selection rules for the quantum numbers:

1. VIBRATIONAL-ELECTRONIC TRANSITION

    $\Delta v = 0, \pm 1, \pm 2, \ldots$ for the anharmonic oscillator.

2. ROTATIONAL-ELECTRONIC TRANSITION

    In the symmetric-top model, $\Delta J = \pm 1$ if $\Omega = 0$ in both upper and lower states, and $\Delta J = 0, \pm 1$ (excluding $J = 0 \leftrightarrow J = 0$) if at least one of the two states has $\Omega \neq 0$.

3. ELECTRONIC TRANSITION

    $\Delta\Omega = 0, \pm 1$.

The parity of the wavefunction under inversion must change: g (even parity) ↔ u (odd parity). The parity of non-degenerate wavefunctions upon reflection in a plane of symmetry must not change: $0^+ \not\leftrightarrow 0^-$.

Two-photon resonance processes allow the investigation of electronic states which are symmetry-forbidden in one-photon spectroscopy. The selection rules for two-photon resonance may easily be deduced from the previous results. The allowed change in Ω is 0, ± 1, ± 2. Since the ground electronic state of I_2 has the configuration 0_g^+, the first (non-resonant) state must have symmetry "u" while the second (resonant) state must be of symmetry "g" and therefore is inaccessible via conventional one-photon absorption from the ground state. Starting from the configuration 0_g^+, the I_2 molecule may therefore go to 0_g^+, 1_g, or 2_g. The selection rules for J are $\Delta J = 0$, ± 1, ± 2, giving rise to S, R, Q, P and O branches.

2.5 The Iodine Molecule

Diatomic Iodine, $I_2{}^{127}$ with reduced mass 63.466 amu, has the electronic ground-state configuration 0_g^+ with vibrational and rotational constants as follows (Herzberg, 1950):

$$\omega_e'' = 214.57 \qquad cm^{-1}$$

$$\omega_e \chi_e'' = 0.6127 \qquad cm^{-1}$$

$$\omega_e y_e'' = -0.000895 \qquad cm^{-1}$$

$$\omega_e z_e'' = -0.0000187 \qquad cm^{-1}$$

$$B_e'' = 0.03735 \qquad cm^{-1}$$

$$\alpha_e'' = 0.000117 \qquad cm^{-1}$$

$$D_e'' = 4.5 \quad 10^{-9} \qquad cm^{-1}$$

$$r_e'' = 2.666 \qquad \overset{\circ}{A}$$

Note that D_e'' is calculated using B_e'' and ω_e'' in equation 2.6.

According to the anharmonic oscillator model, the quantized vibrational energy (equation 2.3) of the ground electronic state of diatomic Iodine is given in wavenumber units by:

$$G(v'') = 214.57(v'' + \tfrac{1}{2}) - 0.6127(v' + \tfrac{1}{2})^2$$

$$-0.000895 \ (v'' + \tfrac{1}{2})^3 + 0.0000187 \ (v'' + \tfrac{1}{2})^4 \ .$$

For later use, the energy levels $G(v'')$ plus the first and second differences, $\Delta G(v'')$ and $\Delta^2 G(v'')$, are tabulated for the first six vibrational levels of I_2 in Table I. No isotope effects are expected in the spectrum of Iodine, since the isotope I_2^{127} has abundance better than 99.9% (Robinson, 1974). The quantized rotational energy (equation 2.7) of

v	$\omega_e(v+\frac{1}{2})$ (cm^{-1})	$\omega_e x_e(v+\frac{1}{2})^2$ (cm^{-1})	$\omega_e y_e(v+\frac{1}{2})^3$ (cm^{-1})	$\omega_e z_e(v+\frac{1}{2})^4$ (cm^{-1})	G(v) (cm^{-1})	ΔG(v) (cm^{-1})
0	107.29	-0.1532	-0.0001	-	107.14	
						213.34
1	321.86	-1.379	-0.0030	0.0001	320.48	
						212.11
2	536.43	-3.829	-0.0140	0.0007	532.59	
						210.87
3	751.00	-7.506	-0.0384	0.0028	743.46	
						209.63
4	965.57	-12.41	-0.0816	0.0077	953.09	
						208.39
5	1180.14	-18.53	-0.1489	0.0171	1161.48	
						207.13
6	1394.71	-25.89	-0.2458	0.0334	1368.61	

$$\Delta^2 \simeq 1.24 \text{ cm}^{-1}$$

Table I . Vibrational Energy Levels of the Ground Electronic State of I_2.

the ground electronic state is given in wavenumber units by:

$$F_v(J") = \left[0.03735 - 0.000117 \left(v" + \frac{1}{2} \right) \right] J"(J" + 1)$$

$$- 4.5 \times 10^{-9} J"^2 (J" + 1)^2 . \qquad (2.13)$$

The ionization potential of molecular Iodine is 75,814 ± 10 cm^{-1} (Myer and Samson, 1970, and Venkateswarlu, 1970). The aim of this research is to obtain multiple-photon ionization of the I_2 molecule via the reaction:

$$I_2 + Nv \rightarrow I_2^+ + e^- ,$$
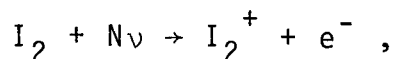
where N is the number of photons absorbed simultaneously by I_2 in the photoionization process. The fundamental frequency v of the incident light must lie within the spectral range 3600-7400 Å (27,778 - 13,514 cm^{-1}) provided by commercial laser dyes available to date. The requirement

$$13,514 \text{ cm}^{-1} \leqslant v \leqslant 27,778 \text{ cm}^{-1}$$

$$\text{with } Nv \geqslant 75,814 \pm 10 \text{ cm}^{-1}$$

is satisfied for the values N = 3, 4, 5 and 6. Since the lowest-order nonlinearity will be the most intense, we choose N = 3. The photoionization reaction is then

$$I_2 + 3v \rightarrow I_2^+ + e^- ,$$
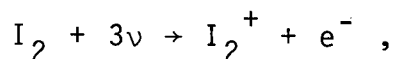
where the exciting energy required is $v \geqslant 25,271 \pm 3$ cm^{-1} which corresponds to photons of wavelength $\leqslant 3957 \pm 1$ Å.

In principle, non-linear photodissociation of I_2 contributes to the non-linear photoelectron signal. Since the ionization and dissociation thresholds are similar, the onset of dissociation occurring at approximately 71,300 cm^{-1} (Myer and Samson, 1970), both processes will occur in the same order of non-linearity. The reaction

$$I_2 + 3\nu \rightarrow I_2^* \rightarrow I^+ + I^-$$
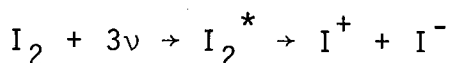
will contribute only a very small percentage, however, since the photodissociation yield falls below 10%, compared to a photoionization yield of 80-100% (Myer and Samson, 1970), throughout the spectral range investigated.

In order that the incident light energy not be lost through linear absorption and scattering, the wavelength of the incident light must not coincide with a resonant state in diatomic Iodine (section 2.1). According to previous investigations of diatomic Iodine (Haranath and Rao, 1958, Mathieson and Rees, 1956, Mulliken, 1934 and 1971, Nobs and Wieland, 1966, and Venkateswarlu, 1970), there appear numerous band systems in the visible and near-ultraviolet absorption spectra (single-photon) of I_2. No bands appear, however, in absorption from the ground state between the wavelengths 3957 Å, the longest wavelength possible for triple-photon ionization of I_2, and 3600 Å, the lower limit of the dye laser. Thus, if a laser dye is chosen which lases below 3957 Å, we expect to achieve triple-photon ionization with

no complications from single-photon resonances. When reson-
ant enhancement of the photoionization signal occurs, we
expect two-photon resonance to an intermediate state of
symmetry "g" followed by photoionization.

2.6 Vibrational Analytic Techniques

In the visible and near-ultraviolet spectrum of mol-
ecular Iodine, the band heads are clearly developed
(Venkateswarlu, 1970, and Petty et al., 1975). Since a maxi-
mum of intensity (band head) will occur in each vibrational
band at about the same energy or J value (section 2.8),
rotational energies may be ignored in the vibrational analysis.
Thus, once the vibrational transitions have been assigned,
a simple measurement of the separation of the band heads in
a chosen progression will yield values for the vibrational
constants ω_e, $\omega_e x_e$, etc. for the chosen electronic state,
according to equations 2.4 and 2.5. Furthermore, it will be
demonstrated that the head of any band lies very close to
the band origin (section 4.5), and thus the minimum T_e of
the potential well of the upper electronic state may be found
within a few wavenumbers.

2.7 Franck-Condon Rotational Analytic Techniques

Determination of the rotational constants B_v' and r_e'
through analysis of rotational energies is complex. The
laser's bandwidth ($\simeq$ 0.2 Å) is broader than the linewidth
of a single resonance line in I_2 ($\simeq$ 0.03 Å, essentially the

Doppler width) so that the band is not resolved. To carry
out the rotational analysis, a different approach must be
found than that of measuring the separation of the rotational
energy levels. The measurement of Franck-Condon factors is
an alternative approach with very precise results.

The relative intensity of vibrational-electronic
transitions in absorption is governed by (a) the relative
population of the initial vibrational states of the molecule,
and (b) the overlap of the probability distribution functions
of the two vibrational states under consideration. The first
factor is $e^{-G_0(v'')/(0.6952 \text{ cm}^{-1}/°K)T}$ as discussed in section
2.2.2. The square of the second factor, the overlap integral,
is termed the Franck-Condon factor of the states, and depends
upon the relative equilibrium positions r_e' and r_e'' and the
relative vibrational frequencies ω_e' and ω_e'' of the elec-
tronic states. When three of these molecular constants are
known the fourth may be calculated from a measurement of
the relative band intensities. Since the rotational constant
of the excited electronic state obtained in Iodine was dif-
ficult to measure, the Franck-Condon factors were used to
determine the size of the molecule in the upper electronic
state. The one assumption of this approach is that the
ionization probability from the resonant excited state is
independent of v'.

We may approximate the lowest-lying vibrational states
with the eigenfunctions of the harmonic oscillator model.

These are the Hermite orthogonal functions (Herzberg, 1950).
The normalized vibrational wavefunction in the ground elec-
tronic state is then:

$$\psi_{v''}(x) = \left(\frac{\alpha}{\pi}\right)^{\frac{1}{4}} \frac{1}{2^{v''/2} \sqrt{v''!}} e^{-\alpha x^2/2} H_{v''}(\sqrt{\alpha}x)$$

where x is the distance from the equilibrium separation of
the nucleii, $\alpha = \mu\omega_e''/\hbar$, and $H_{v''}(\sqrt{\alpha}x)$ is a Hermite poly-
nomial of v'-th degree. In the excited electronic state the
normalized vibrational wavefunction is:

$$\psi_{v'}(y) = \left(\frac{\beta}{\pi}\right)^{\frac{1}{4}} \frac{1}{2^{v'/2} \sqrt{v'!}} e^{-\beta y^2/2} H_{v'}(\sqrt{\beta}y)$$

where y is the distance from equilibrium and $\beta = \mu\omega_e'/\hbar$.
The Hermite polynomials are obtained from the generating
function $H_n(u) = (-1)^n e^{u^2} (d^n/du^n) e^{-u^2}$. The Franck-Condon
factor between states v' and v'' is:

$$F(v',v'') = \left[\int_{\infty}^{\infty} \psi_{v''}(x) \, \psi_{v'}(x-\partial) \, dx \right]^2$$

where ∂ represents the distance between the equilibrium
positions in the ground and excited electronic states.

The method of evaluating the overlap integrals is that
of Pryce (1976), in which a generating function was derived
whose coefficients are proportional to the overlap integrals
between the different vibrational states. The Franck-Condon

factors take the form:

$$F(v',v") = \frac{(v'!)\,(v"!)}{2^{(v'+v")}} \ P \ e^{-PD^2/2} \Big(G(v',v")\Big)^2$$

where $G(v',v")$ is the coefficient of $s^{v'}t^{v"}$ in the expansion of the generating function $H(s,t)$:

$$H(s,t) = e^{-Q'Ds}\ e^{Q"Dt}\ e^{2Pst}\ e^{Rs^2}\ e^{-Rt^2}\ .$$

The quantities P, R, Q' and Q" are constants for any two given electronic states, while D varies with the separation of the equilibrium positions in the upper and lower electronic states. The definitions are:

$$\eta = \tfrac{1}{2}\ln(\omega'/\omega")$$

$$P = \operatorname{sech}\eta$$

$$R = \tanh\eta$$

$$Q' = e^{-\eta/2}\operatorname{sech}\eta$$

$$Q" = e^{\eta/2}\operatorname{sech}\eta$$

$$D = \partial\,\sqrt{m/h}\ \ (\omega'\omega")^{\tfrac{1}{4}}$$

The first few coefficients $G(v',v")$ are:

$$G(0,0) = 1$$

$$G(1,0) = -Q'D$$

$$G(2,0) = \tfrac{1}{2}Q'^2D^2 + R$$
$$\vdots$$

$$G(1,1) = 2P - Q'Q"D^2$$

$$G(2,1) = -2PQ'D + \tfrac{1}{2}Q'^2Q"D^3 + RQ"D$$
$$\vdots$$

$$G(2,2) = 2P^2 - R^2 + \tfrac{1}{2}RQ"^2D^2 - \tfrac{1}{2}RQ'^2D^2 - 2PQ'Q"D^2$$
$$+ \tfrac{1}{4}Q'^2Q"^2D^4$$
$$\vdots$$

- 34 -

2.8 Electronic Configuration and Band Contour

In the three-step ionization of I_2, arising from a
resonant two-step transition from the X 0_g^+ state to some
intermediate even-parity state, followed by non-resonant
ionization, it would be useful to have firm theoretical
prediction concerning the intensities associated with the
rotational structure. The intensities of the individual
rotational members within a given vibrational band are
proportional to three factors: (a) a Boltzmann factor
$e^{-F_v(J'')hc/kT}$, (b) the frequency ν of the transition, and
(c) the transition probability between the two rotational
states. The dependence on the frequency over the range
used in this research may be neglected, since the variation
is only 4%. The transition probability is that part of
$\langle \psi_g^o | \vec{M} | \psi_m^o \rangle^2$ which depends on J' and J", and is represented
by analogues to the Hönl-London factors appearing in one-
photon absorption. Since I_2 is a heavy molecule, high rotat-
ional quantum numbers are encountered, even in the vicinity
of the band peak, and the analogues to the Hönl-London factors
may be used in their approximation for large J. These factors
are asymptotically multiples of (2J+1), the statistical
weighting factor of the rotational states. Thus the trans-
ition probability is essentially constant in each branch.
The intensity distribution within a rotational branch there-
fore resembles closely the population distribution of the

initial rotational states:

$$i(J) = C(2J+1) \, e^{-F_v(J'')hc/kT}.$$

The rotational term $F_v(J'')$ of equation 2.7 simplifies since the symmetric-top term $(A'' - B_v'')\Omega''^2$ vanishes in the ground electronic state of I_2, and since the small correction term D_v'' is negligible $(\approx 10^{-7} \, B_v'')$. The relative intensity of the transitions of any single branch is then described by $(J \equiv J'')$:

$$i(J) = C(2J+1) \, e^{-B_v''J(J+1)hc/kT}.$$

Since the bands of Iodine are unresolved, the intensity distribution may be treated as an essentially continuous function of J.

The contour of a single branch may be determined by convoluting the intensity distribution $i(J)$ with the laser spectrum, approximated as a square-topped wave 1.5 cm^{-1} wide. The contour $I(\nu_\ell)$ of a branch expressed as a function of laser frequency is:

$$I(\nu_\ell) = \int_{J_1}^{J_2} i(J) \, dJ$$

$$= \left. \frac{-kT}{hcB_v''} \, e^{-B_v''J(J+1)hc/kT} \right|_{J_1}^{J_2}$$

$$= a(e^{-J_1(J_1+1)/a} - e^{-J_2(J_2+1)/a})$$

where $a = kT/hcB_v''$.

The limits of integration are determined by the laser band-width. Thus:

$$J_2 = J(\nu_\ell + 0.75 \text{ cm}^{-1}) \text{ ,}$$

$$\text{and} \quad J_1 = J(\nu_\ell - 0.75 \text{ cm}^{-1}) \text{ .}$$

The limits of integration for each branch may be deduced from equations 2.14 to 2.17. Placing the zero of ν_ℓ at $\nu_o/2$, the results are as follows for the case $|\Delta B| << B_v'$:

O-BRANCH

$$J_O = \frac{2B_v'}{\Delta B} \pm \sqrt{\left(\frac{2B_v'}{\Delta B}\right)^2 + \frac{2\nu_\ell - 2B_v'}{\Delta B}} \qquad (2.14)$$

P-BRANCH

$$J_P = \frac{B_v'}{\Delta B} \pm \sqrt{\left(\frac{B_v'}{\Delta B}\right)^2 + \frac{2\nu_\ell}{\Delta B}} \qquad (2.15)$$

R-BRANCH

$$J_R = -\frac{B_v'}{\Delta B} \pm \sqrt{\left(\frac{B_v'}{\Delta B}\right)^2 + \frac{2\nu_\ell - 2B_v'}{\Delta B}} \qquad (2.16)$$

S-BRANCH

$$J_S = -\frac{2B_v'}{\Delta B} \pm \sqrt{\left(\frac{2B_v'}{\Delta B}\right)^2 + \frac{2\nu_\ell - 6B_v'}{\Delta B}} \qquad (2.17)$$

The contour of the Q-BRANCH is simply:

$$I_Q(\nu_\ell) = 2a \sinh\left(\frac{1.5}{a\Delta B}\right) e^{-2\nu_\ell/a\Delta B} \text{ .}$$

The requirement that J be real and positive places restrictions upon the ν_ℓ for which there are contributions to the intensity.

Prediction of the band contours for the various electronic configurations possible in the resonant state requires a knowledge of the relative branch intensities. For a given electronic configuration it is necessary to sum over all possible intermediate electronic states to arrive at the two-photon analogues to the Hönl-London factors. The calculations were carried out by Pryce (1976) with the following results:

Transition Branch	$0_g^+ \rightarrow 0_g^+$	$0_g^+ \rightarrow 1_g$	$0_g^+ \rightarrow 2_g$
O	$\dfrac{J(J-1)}{(2J-1)}(\alpha-\beta)^2$	$\dfrac{J(J-2)}{(2J-1)}$	$\dfrac{(J-2)(J-3)}{4(2J-1)}$
P	0	$\tfrac{1}{2}(J+1)$	$\tfrac{1}{2}(J-2)$
Q	$(2J+1)\left[\dfrac{2J(J+1)(\alpha-\beta)^2}{3(2J-1)(2J+3)}+\dfrac{5}{6}(\alpha+2\beta)^2\right]$	$\dfrac{3(2J+1)}{2(2J-1)(2J+3)}$	$\dfrac{3(J-1)(J+2)(2J+1)}{2(2J-1)(2J+3)}$
R	0	$\tfrac{1}{2}J$	$\tfrac{1}{2}(J+3)$
S	$\dfrac{(J+1)(J+2)}{(2J+3)}(\alpha-\beta)^2$	$\dfrac{(J+1)(J+3)}{(2J+3)}$	$\dfrac{(J+3)(J+4)}{4(2J+3)}$

In the $0_g^+ \rightarrow 0_g^+$ transition, α and β are contributions from

intermediate 0_u^+ and 1_u states respectively, normalized so that $3\alpha^2 + 4\alpha\beta + 8\beta^2 = 1$. The relative branch strengths may, for large rotational energies, be expressed independently of J as follows:

(1) For $0_g^+ \rightarrow 0_g^+$ the R and P branches are totally absent, and O:Q:S = 3:2+x:3 where x is a positive quantity whose actual value depends on details of the intermediate states. The extreme band contours are 3:2:3 and a contour which is entirely Q-like.

(2) For $0_g^+ \rightarrow 1_g$ the Q branch is absent and the other branches are all equally strong. O:P:Q:R:S = 1:1:0:1:1.

(3) For $0_g^+ \rightarrow 2_g$ the ratios are O:P:Q:R:S = 1:4:6:4:1.

Once the rotational analysis has been carried out, the band contour for each electronic configuration may be predicted by summing the contributions of all branches. All bands of a vibrational progression would be similar in contour.

It is noteworthy that for very large J, all band configurations become Q-like (pure exponential):

$$I(\nu_\ell) \propto e^{-2\nu_\ell / a\Delta B} .$$

In a plot of $\ln(I)$ against ν_ℓ we may determine ΔB from the slope at high energy. The method in inherently approximate, but will serve to check the Franck-Condon rotational analysis.

3. INSTRUMENTATION AND EXPERIMENTAL DESIGN

3.1 Introduction

The light source used to photoionize the Iodine was a Molectron DL-300 tunable dye laser pumped by a UV-1000 nitrogen laser, which provided 5-nsec pulses of bandwidth 0.2$\overset{o}{A}$. A digital grating drive mechanically tuned the laser. Triple-photon ionization of the I_2 molecule requires an exciting energy $\geq$ 25,271 $\pm$ 3 cm^{-1} (section 2.5), which corresponds to photons of wavelength $\leq$ 3957 $\pm$ 1$\overset{o}{A}$. The laser dye chosen was Butyl PBD in the solvent p-dioxane which lases over 3650-3800$\overset{o}{A}$; this dye provides the highest output power available at present in this region of the spectrum.

The laser beam was focused with a 9 3/4 cm quartz lens between the electrodes of a glass cell containing Iodine vapor at its saturated vapor pressure (Figure 1). Great sensitivity was achieved by focusing the laser very close to the negative electrode in order to accelerate the product electrons over the longest possible distance. An oven was built to house the Iodine cell for the production of high-temperature spectra.

The simultaneous monitoring of a small portion of the laser output along with the photoionization signal was required both for calculation of the wavenumbers of the band heads and for determination of the relative band intensities. Thus a beam splitter of low reflectivity was required immed-
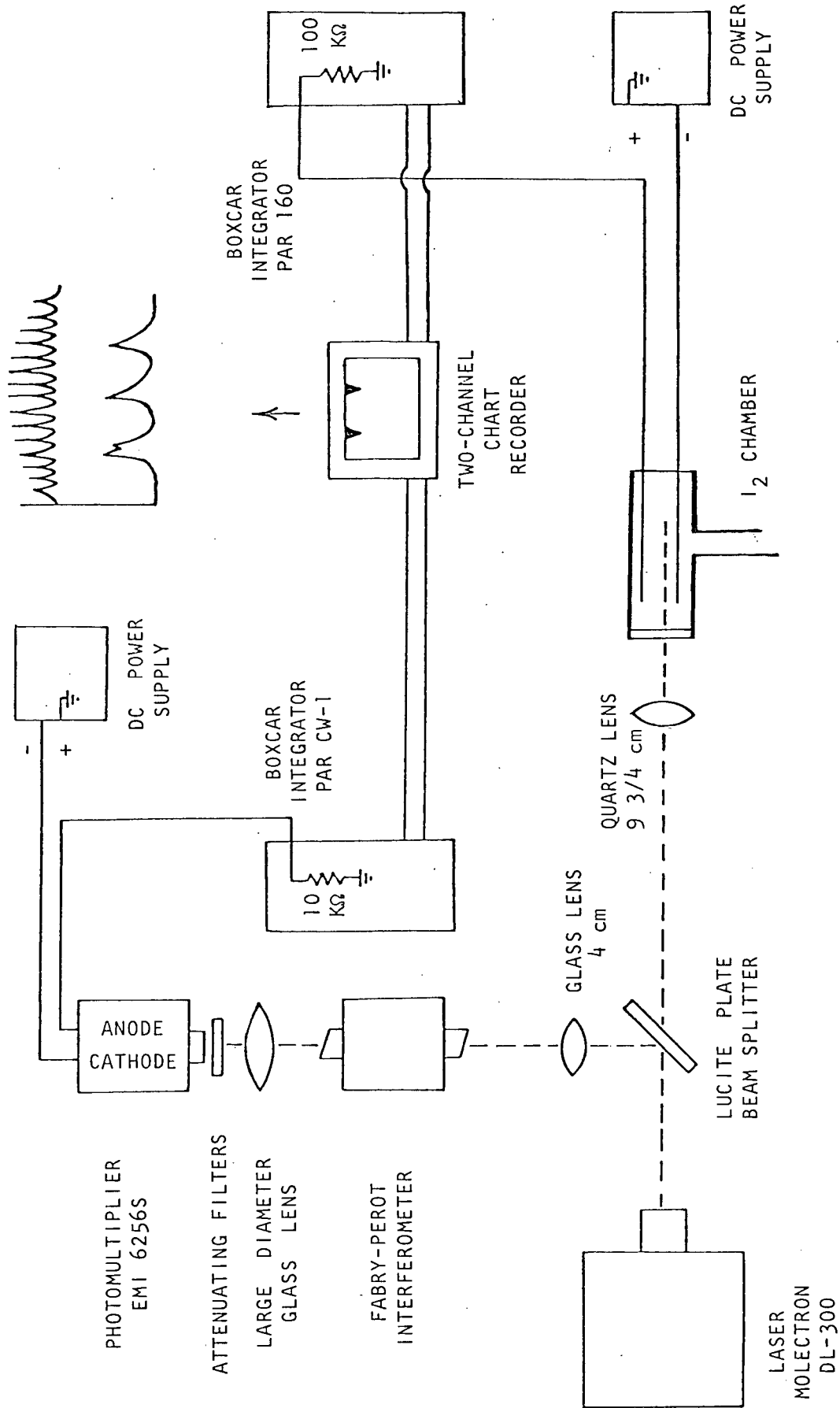
Figure 1. The Apparatus

iately in front of the laser. A lucite plate of thickness 4.3 mm served well. To facilitate determination of the relative band intensities, the direct reflected laser light was measured with photomultiplier tube EMI 6256S. Attenuating materials were used to shield the photocathode in order to eliminate optical saturation of the photomultiplier. These materials, namely a high-neutral-density filter and one, and in some cases two, sheets of diffusing glass, provided an attenuation on the order of 10^6 (Appendix A). A Fabry-Perot interferometer was introduced into the path of the reflected beam (Figure 1) as a very accurate means of measuring the wave-number separation of the photoionization-band heads. The plate separation was adjusted to 0.05020 cm; the gap between the plates was at atmospheric pressure. As the laser was tuned, the interferometer provided closely-spaced fringes whose separation could be accurately calibrated. A 4 cm glass lens was used to expand the beam to fill roughly 7 cm^2 of the interferometer plate. A second, large-diameter glass lens collected the light from the interferometer and focused the center of the fringes on a pinhole in aluminum foil pre-ceeding the attenuating filters of the photomultiplier.

The pulsed signals from the photomultiplier and the Iodine cell were fed to two separate boxcar integrators, each triggered by the synchronous output of the nitrogen laser. The boxcar integrators converted the repetitive

waveforms to dc signals consisting of the time-average of a number of pulse peaks, the number determined by the signal-to-noise improvement desired. The boxcar outputs were displayed in analogue form on a two-channel chart recorder.

Fused quartz was employed in critical places, for example in the window of the photomultiplier tube, in the lens focusing the laser beam into the Iodine cell, and in the window of the oven, since the transmission is excellent [98.9% at 1 cm (Koller, 1965)] far into the ultraviolet.

The operating characteristics and calibration of the major pieces of apparatus is described in the following section.

3.2 Calibration and Operating Characteristics

3.2.1 Laser

The light source was a state-of-the-art Molectron DL-300 pulsed tunable organic dye laser, whose engineering design follows Hänsch (1972) pumped by a UV-1000 nitrogen laser at 3371 Å. The laser provides 5-nsec pulses at repetition rates anywhere between 5 and 50 pps, the highest time-averaged power output occurring at the rate 10 pps. The discharge channel design of the nitrogen laser delivers a peak power of 1 MW per pulse at 10 pps. The dye laser is designed to allow dye interchange, thus achieving the wide tuning range of 3600-7400Å, for which the output power depends upon the particular dye and solvent chosen. A high dis-

persion echelle grating in Littrow mount functions as a wave-length-selective end reflector in the dye laser cavity. Tuning of the dye laser is accomplished by a simple rotation of the grating. In the absence of a Fabry-Perot intercavity etalon, the bandwidth of the dye-laser output is approximately 0.2Å, or 1.5 cm^{-1} at 3750Å. This bandwidth may in practice be slightly narrower due to the third-power dependence of the photoelectron signal. The beam divergence is 2 mrad. An intercavity beam expanding telescope together with the high quality diffraction grating provides excellent wavelength reproducibility (0.01Å) from shot to shot. Amplitude stability is also ensured from shot to shot by using an automatic stirrer, magnetically driven, to circulate the liquid dye in a 2 cm^3 cell, in order to return the dye to optical homogeneity before the arrival of the next pump pulse. The amplitude is not stable over the long term, however, as photodissociation within the dye solution both decreases the dye concentration and introduces impurities in the form of dissociation products.

Molectron recommends, after Hänsch (1972), the relatively high concentration of dye in solvent of 5 x 10^{-3} mole/liter as being insensitive to small amounts of impurities or to dye decomposition. With a molecular weight 354.45 gm/mole, 3.54 mg of the organic dye Butyl PBD are required in 2 cm^3 of solvent. At this concentration, the lifetime of a sample of Butyl PBD in p-dioxane is approximately six hours of continuous use at 10 pps. The peak power obtained

from a fresh sample of dye is 20 x 10^{-5} joules per pulse, or 40 KW per pulse, at 3760$\overset{o}{A}$. The emission curve over the useful range 3650-3800$\overset{o}{A}$ is given in Figures 10 and 11. Note that the emission varies with the age of the dye.

It is conceivable that the output angle of the laser beam changes slightly as the laser grating is rotated. This was of no practical concern, however, as it was experimentally determined that the intensity of the photoelectron signal is insensitive to small rotations of the Iodine chamber.

3.2.2 Scanning System

A mechanical scanning system for the grating of the dye laser was assembled, as a means of changing the laser's wavelength in a continuous and smooth manner. Synchronous stepping motor HS50 and the accompanying translator module STM1800C (manufactured by SLO-SYN) were used for this assembly.

The translator module is a plug-in printed circuit board with logic capabilities for driving a SLO-SYN motor in stepping applications. Bidirectional operation of the motor is possible at rates up to 2000 steps per second. The external triggering pulse requirement is an 8 to 10 volt negative change of voltage, and a minimum pulse width of 30 μsec.

The translator module requires a power supply which can provide -25 volts dc and + 12 volts dc with a maximum ripple of 5%. The circuit diagram of the power supply which was built is given in Figure 2 (Millman and Halkias, 1972).

The wiring connecting the SLO-SYN motor to the translator module is shown in Figure 3. Two heavy-duty 5.5Ω current-limiting resistors (shown as R in the Figure) are required to interface the motor and translator. The resistors used are ten-ohm variable resistors reduced to the required 5.5Ω within about $\pm5\%$, and are rated at 225 watts.

The wavelength increment produced by the digital scanning system in this particular application was $0.00383\overset{o}{A}$ per step over the range 3650-$3800\overset{o}{A}$. Since the laser's bandwidth was roughly $0.2\overset{o}{A}$, an essentially continuous output was achieved. The wavelength increment is calculated as follows. The step angle of the SLO-SYN motor is 1.8^{o} so the motor shaft makes 200 steps per revolution. One revolution of the grating crank advances the laser's wavelength by $100\overset{o}{A}$ in first order. Since the diffraction order appropriate to the dye used in this research is seven, one revolution of the crank is equal to $14.3\overset{o}{A}$. Thus, when the motor drives the grating directly, each step advances the wavelength by $0.0715\overset{o}{A}$, not very much smaller than the laser bandwidth. By using a system of four gears, however, the step size was reduced by a factor $(64/32) \times (112/12) = 18.7$ to the value $0.00383\overset{o}{A}$ per step (3740 steps per revolution). Molectron specifies that the smallest step possible for the grating crank of the dye laser before losing accuracy due to slippage corresponds to a stepping speed of 400 steps per revolution (Reynolds, 1974).
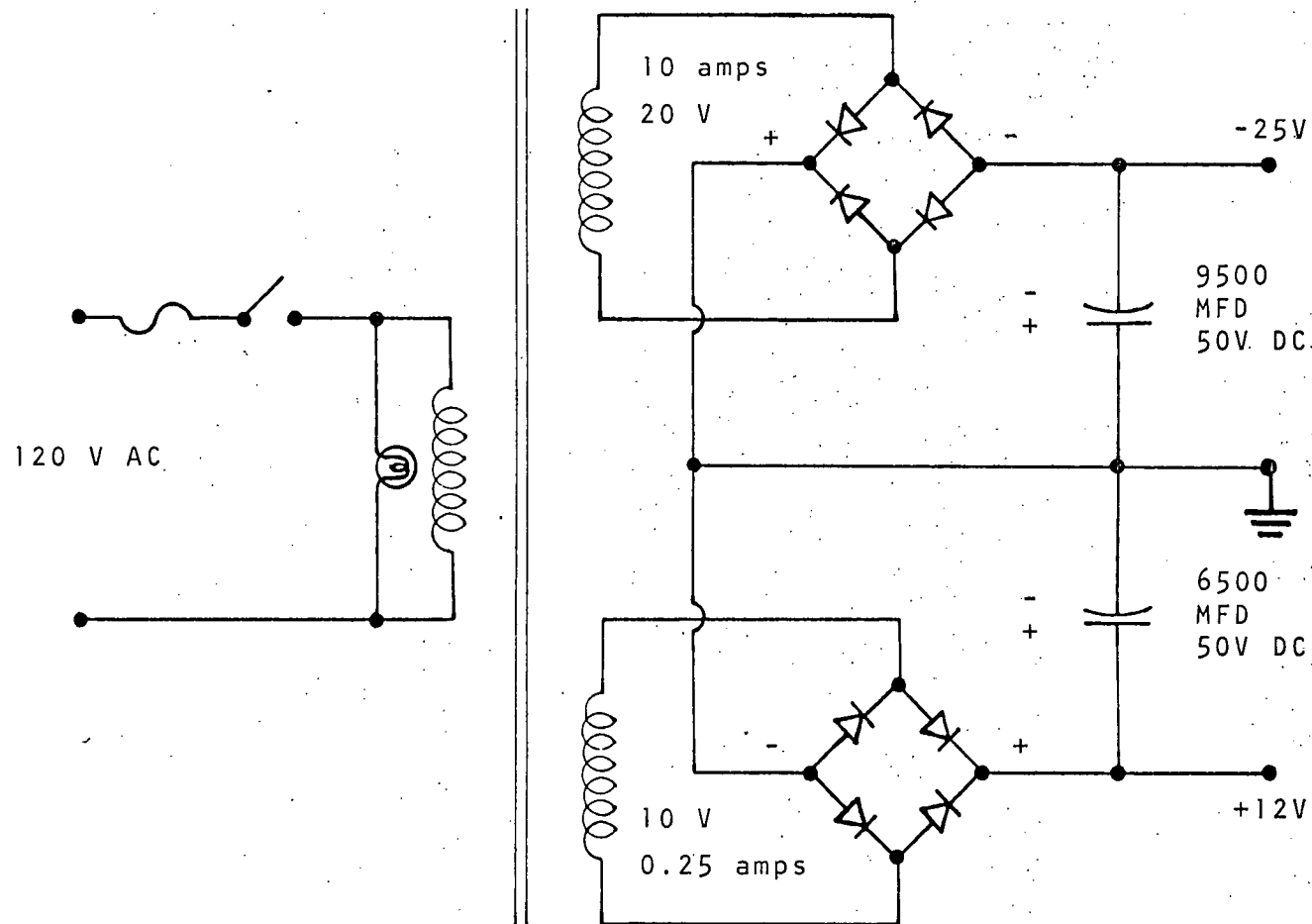
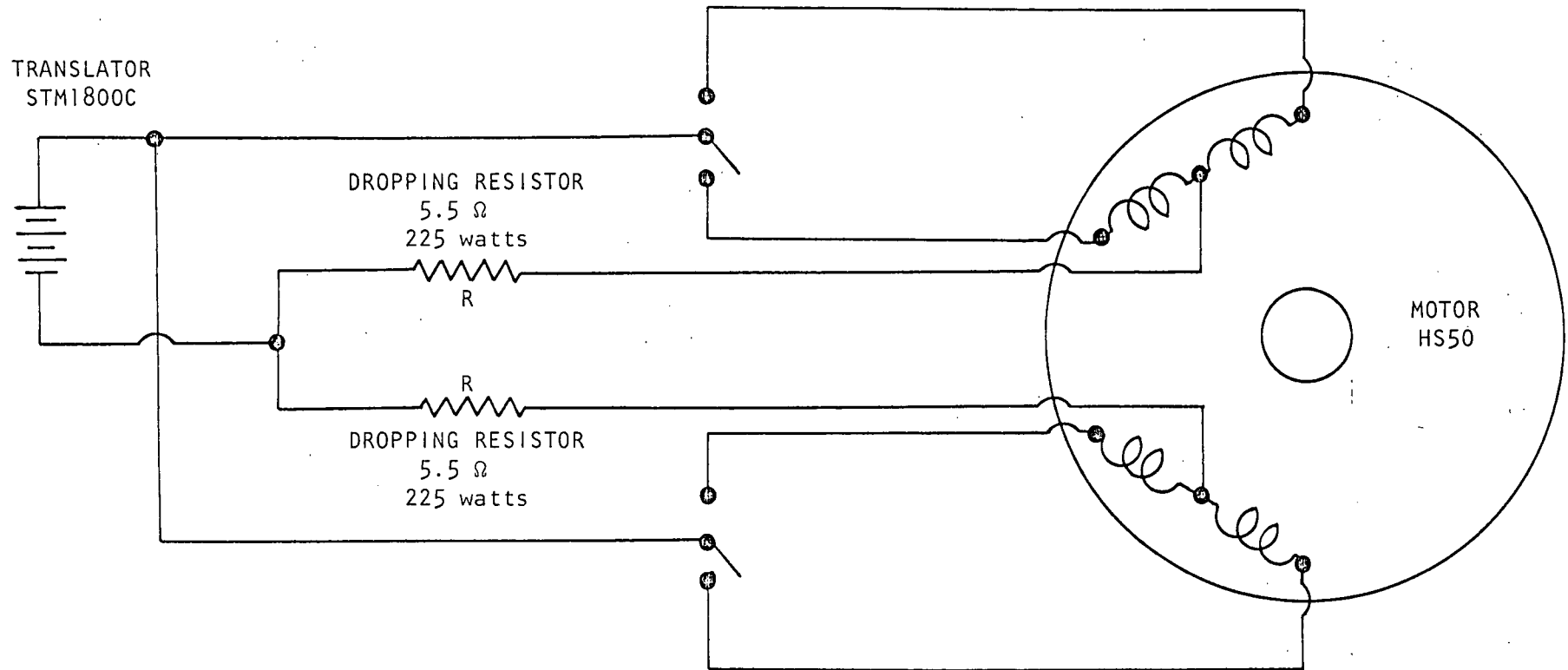Figure 2.   Circuit Diagram of SLO-SYN Translator DC Power Supply

TRANSLATOR
STM1800C

DROPPING RESISTOR
5.5 Ω
225 watts
R

R
DROPPING RESISTOR
5.5 Ω
225 watts

MOTOR
HS50

Figure 3.   SLO-SYN Synchronous Motor Wiring Diagram

After careful adjustments, however, this quoted performance limit was exceeded by a factor of ten. The quality of the scanning system is indicated in the Fabry-Perot interference fringes of Figure 12, where only occasional slippage is apparent.

3.2.3 Iodine Chamber

The glass cell containing Iodine vapor in which the photoionization occurred is shown in Figure 1. The 2 mm pyrex window through which the laser beam entered the cell has a virtually constant transmission of 92% ± 1% over 3650-3800Å, the spectral range of interest (Koller, 1965). The laser beam was focused between parallel-plate electrodes separated by 1.1 cm. A Fluke 415B H.V. dc power supply was used to maintain the electrodes at a constant potential difference. According to the sensitivity desired, the electrode voltage could be adjusted to any point in the range -200 to -400 V (20°C). Lower voltages did not provide an adequate signal, and higher voltages caused an arc instability. In order to obtain adequate sensitivity at high temperatures, this range had to be exceeded up to -430 V.

The cell was constructed with stainless-steel electrodes after Brackmann (1958), who observed that his Iodine ultra-violet-photon-counters which employed this metal for their electrodes had the longest lifetimes. The tungsten leads project through the glass of our cell through a standard

Stupakoff seal. The cell was evacuated to 10^{-6} torr before the Iodine was distilled into it. The cell was fitted with a long stem containing a reserve supply of solid Iodine so that the vapor pressure inside was always the saturated vapor pressure of Iodine. The length of the stem served to isolate the solid Iodine at a lower temperature than the remainder of the cell when placed inside the oven, to ensure that contamination of the cell window and electrodes did not occur when high temperature spectra were taken.

3.2.4 Oven

The oven used to heat the Iodine cell was constructed of one and one-half inch thick asbestos sheeting, cemented with epoxy (maximum temperature $120^{o}C$). The direct current power supply to the heating element was a Sorenson NOBATRON DCR150-15A which supplies high current at low voltage. In this oven the temperature stability was within $0.2^{o}C$ over one hour's operation.

It was important to prevent solid Iodine from depositing on the cell window and electrodes. Thus the oven was designed with two compartments in order to isolate the supply of solid Iodine in the stem of the cell at a lower temperature than the remainder of the cell. The upper compartment has inner dimensions 5 3/4" x 5 3/4" x 6". The laser beam entered through a 1.5 inch diameter aperture covered with a quartz plate to minimize heat loss. The lower compartment

which houses the stem of the cell has inner dimensions
1½" x 4" x 4". The heating element for the oven is Nichrome
wire at seven ohms per foot wound many times around the in-
terior. The length of Nichrome wire in the upper compart-
ment is 270" and in the lower, 26", for a total of 173Ω.
Since the power dissipated per unit volume in the upper com-
partment is about 1.3 times that in the lower, the two com-
partments maintain a sufficient temperature difference even
though the upper one must necessarily sustain a greater heat
loss. From tests done on the empty oven, the temperature in
the upper compartment is about 1.13 times that in the lower
over the range 22° - 100°c.

3.2.5 Photomultiplier

EMI tube 6256S used to monitor the laser intensity is
a 1 cm cathode, 13-stage photomultiplier with fused-quartz
window. With a rise time of 7 nsec and a capacity for peak
currents up to 300 mamp, this tube is adequate for pulsed
operation. The end-window, semi-transparent photocathode and
the venetian-blind type dynodes are coated with CsSb which
has a flat response curve over the spectral range 3650-3800$\overset{\circ}{A}$
of laser dye PBD. The quantum efficiency in this range is
0.13 ± 3%. The noise characteristics are good. Tube 6256S
is designed to have very low anode dark current, less than
0.5 mμamp at -1000 volts. A mu-metal shield was used to pro-
tect the detector from stray magnetic fields. The dc voltage

applied to the photocathode, typically on the order of -600 V, was supplied by Regulated H.V. Supply RE-1602 (Northeast Sc. Corp.).

For good linearity and gain stability, the current drawn from the power supply by the dynodes must not materially change the voltage between the dynodes. This requirement means that this anode current I_a must be considerably smaller than the bleeder current I_b through the potential divider. A good rule of thumb is that $I_a \leq I_b/10$. Pulses of large amplitude may be accommodated providing that by-pass capacitors are used between the last few stages, where the currents are greatest, and providing that the <u>mean</u> anode current $<I_a>$ satisfies the above requirement. Measurement of the laser's intensity involved pulses of large amplitude and very short duration, and to this end chain resistors were chosen such that $<I_a>_{max} = I_b/50$, and by-pass capacitors were connected between the last four stages of the photomultiplier circuit (Figure 4). The linearity of the photomultiplier was tested using four identical neutral density filters at wavelength 3760Å, very near the laser's peak intensity. The response is linear, as shown in Figure 5. In order to avoid optical saturation of the photomultiplier, diffusing glass at a distance of 2 cm from the cathode, followed by a high-neutral-density filter, were used to shield the cathode. The total
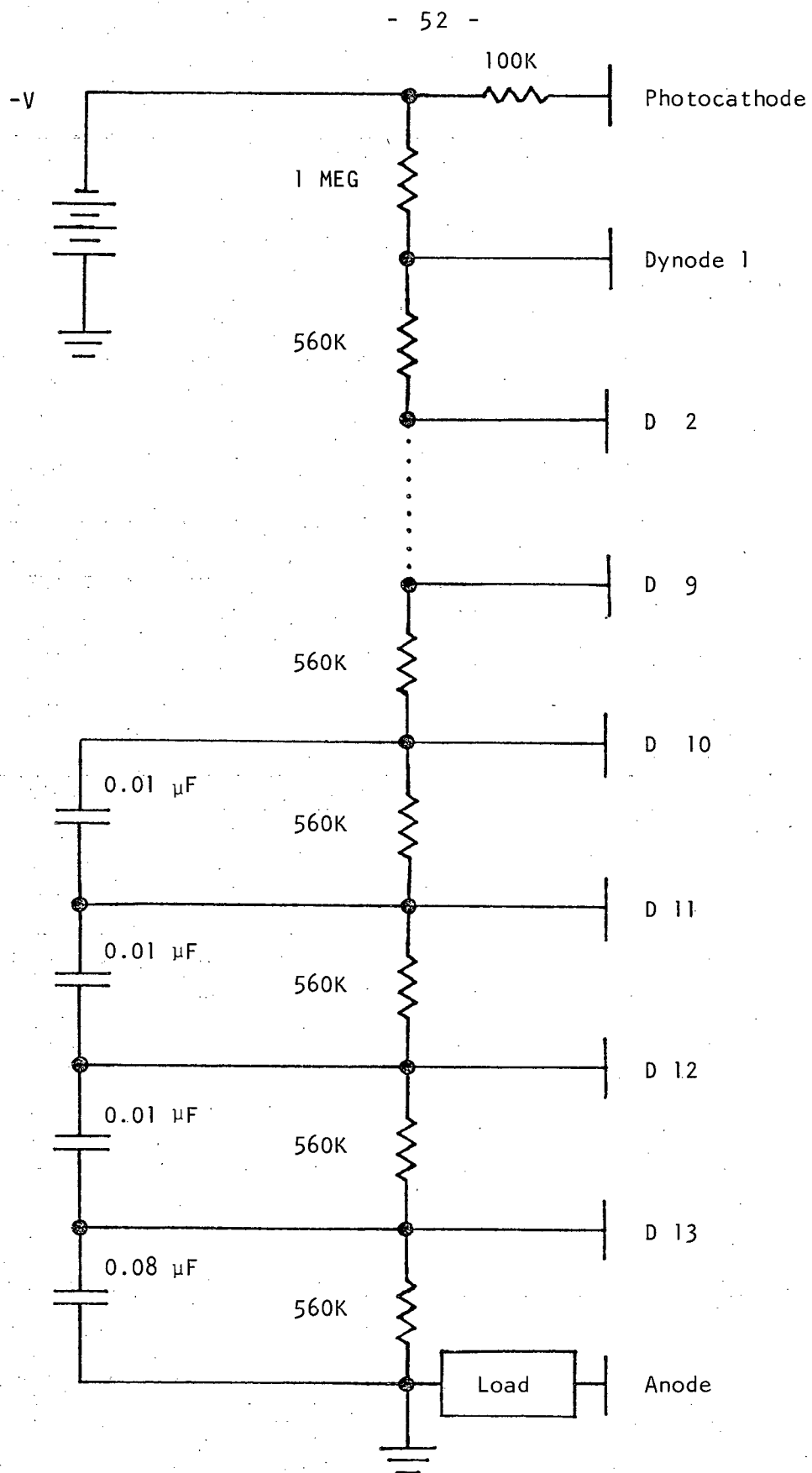
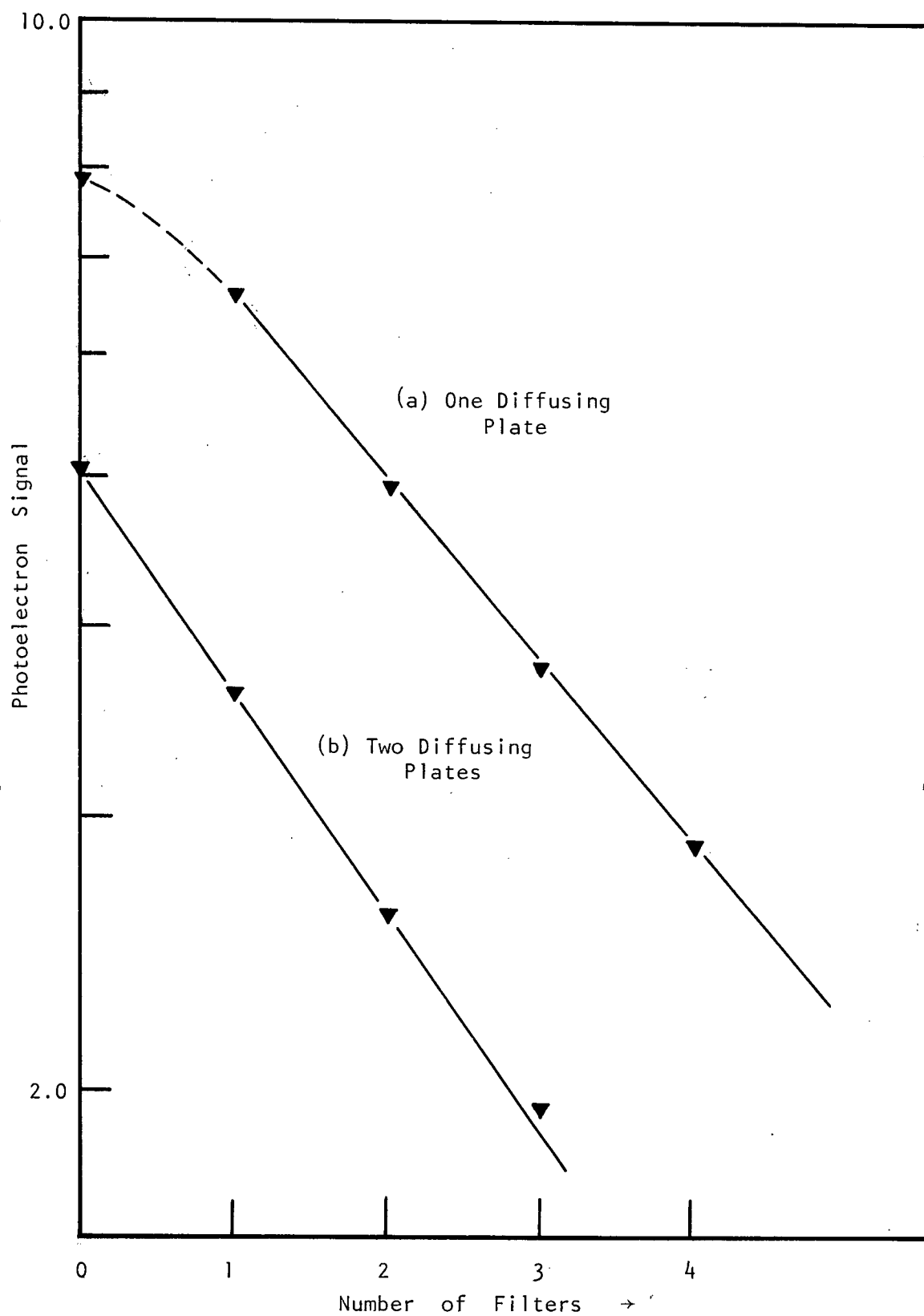Figure 4.   EMI 6256S Photomultiplier Tube Circuit

Figure 5.   Linearity of Photomultiplier Tube EMI 6256S

optical attenuation of these materials as a function of
wavelength is presented in Appendix A.

3.2.6 Boxcar Integrator

Two boxcar integrators were employed: (a) Princeton
Applied Research Model 160, with input impedance 100KΩ in
"normal resolution" mode, and with maximum acceptable input
voltage of 200V peak, was used to process the photoionization
signal, and (b) PAR Model CW-1, with input impedance 10KΩ and
maximum voltage 200V peak, was used to process the signal
from photomultiplier EMI 6256S when this detector was needed.
The purpose of a boxcar integrator is to extract a repetitive
waveform from noise. Since the two signals mentioned above
consisted of repetitive pulses for which the ratio of useful
signal time to dead time was on the order of 10^{-3} to 1 and
10^{-4} to 1 respectively, the boxcar integrator was particularly
useful in our research.

In essence, the boxcar synchronously samples an input
signal using a variable-width, variable-delay gate, which
can be fixed at any point on, or slowly scanned across the
input signal. The boxcar uses negative feedback in an
integrator circuit so that the output asymptotically ap-
proaches the average value of the input signal over the aper-
ture time interval. A trigger pulse which is synchronized with
the external event under study can be applied to the boxcar
to control the timing of the gate. If the gate is fixed on

a single point of the input signal, the boxcar output will rise asymptotically toward the average value of the input signal at the sampled point. If the gate is being scanned across the input signal, the synchronous waveform will be reproduced at the output.

The boxcar is linear to within ±0.25% of full-scale, and has gain stability ±0.5%.

There are two important relationships between the boxcar's control settings. The observed time constant (OTC), which is the real time required for the processed output signal to reach 63% of its final value, and the signal-to-noise improvement ratio (SNIR) are expressed as follows:

$$OTC = \frac{TC}{(f)(AT)} \tag{3.1}$$

$$SNIR = \sqrt{2 \times OTC \times f} \tag{3.2}$$

The control settings are defined as follows:

TC = setting of the time constant dial.

f = pulse repetition frequency.

AT = aperture time, or gate width.

All parameters are valued in sec or sec^{-1}.

3.2.7 Chart Recorder

The model used (Kent) was a two-channel recorder with a wide variety of sensitivity settings. The chart span of ten inches allowed reasonable accuracy in the measurements. A linearity check was performed on two of the sensitivity
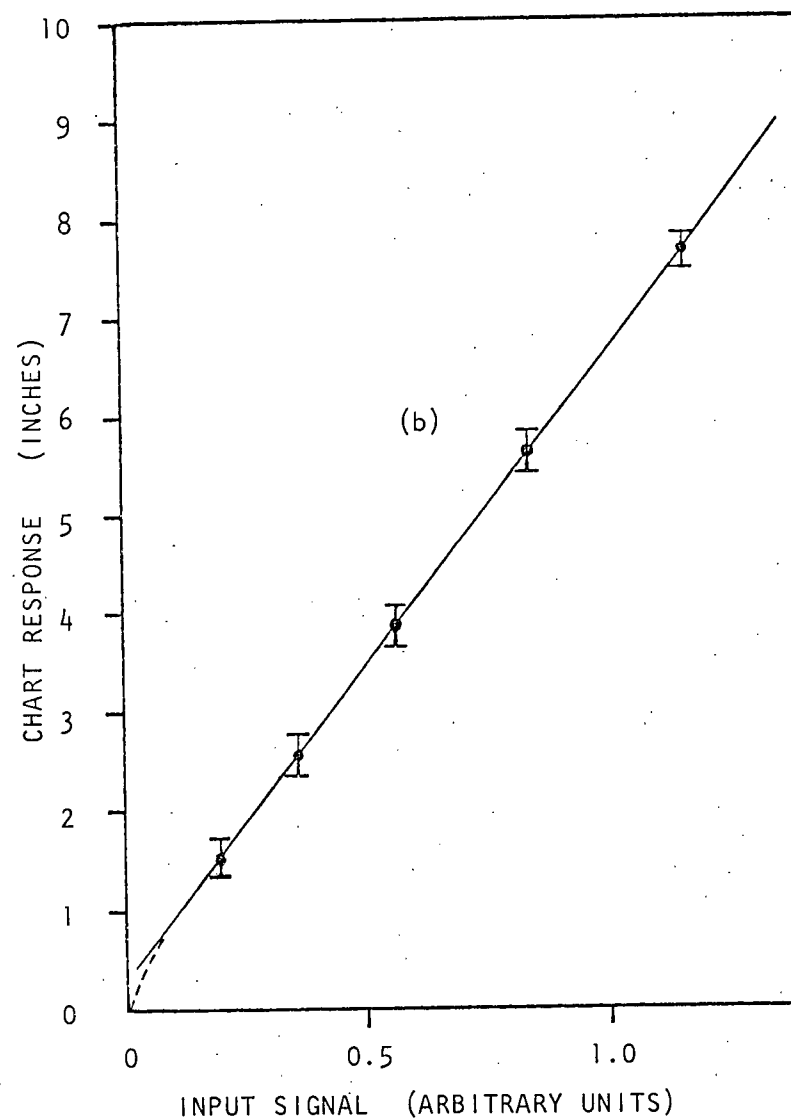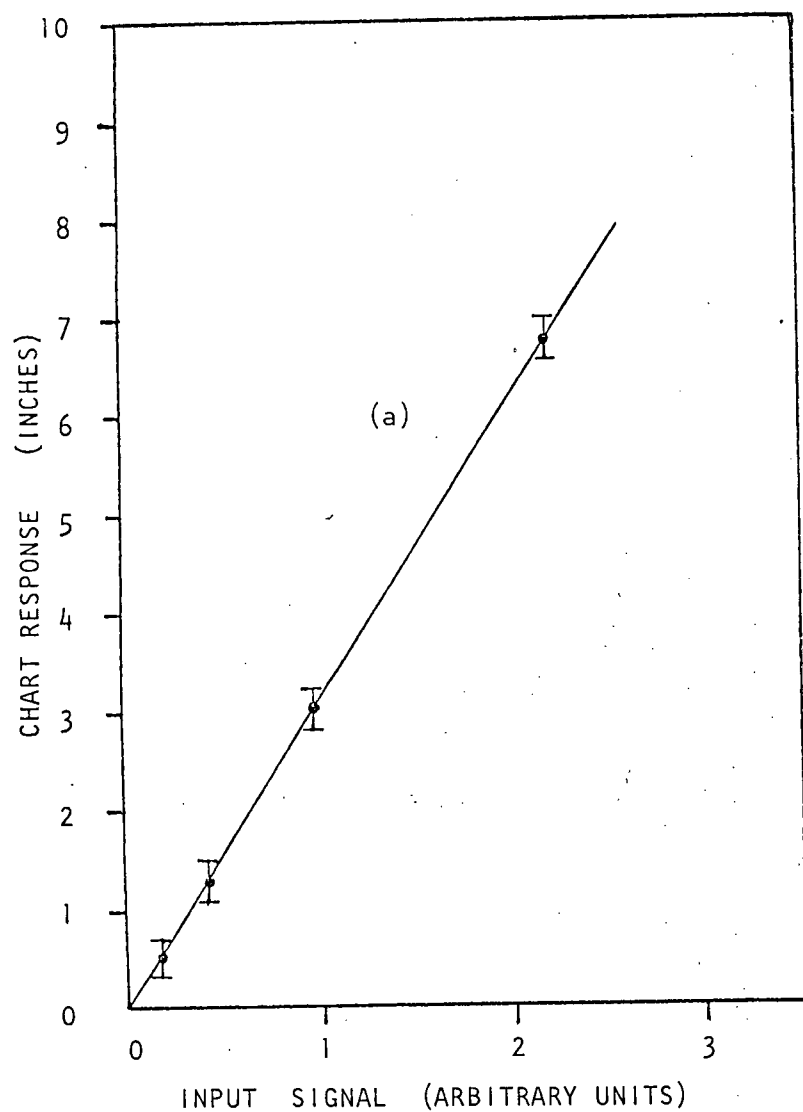
Figure 6.   Test Linearity of Chart Recorder at Two Sensitivity Scales:
(a) 10 Volts Maximum, and (b) 5 Volts Maximum

scales (5 and 10 volts maximum) used most often. Voltage
pulses were fed through boxcar integrator CW-1 and the dc
output was subsequently applied to the chart recorder; the
pulse amplitude was also measured independently on an
oscilloscope. The chart recorder's response to applied
voltage is indicated in Figure 6. Except for the first, and
possibly the last, inch of chart, the response is linear.

3.3 Signal Processing

The processing of the electric signal from the Iodine
chamber was done with boxcar integrator PAR 160. The off-
resonant signal was negligible so that no dc offset was
required in the boxcar integrator or the chart recorder.
The main source of noise in the instruments was electrical
pickup which was reduced by a large extent through careful
shielding. As with any signal averager, the operation of
the boxcar integrator must balance against signal resolution
the signal-to-noise improvement desired. Since a large
signal-to-noise improvement ratio was not required, this could
be sacrificed in order to obtain a resolution of the photo-
ionization bands limited only by the bandwidth of the laser.
With a terminating impedance of 100KΩ on the cell, the signal
pulse had half-width 70 μsec. The pulse shape, reproduced by
the boxcar integrator in the scanning mode, is illustrated in
Figure 7. The aperture width of the boxcar integrator was
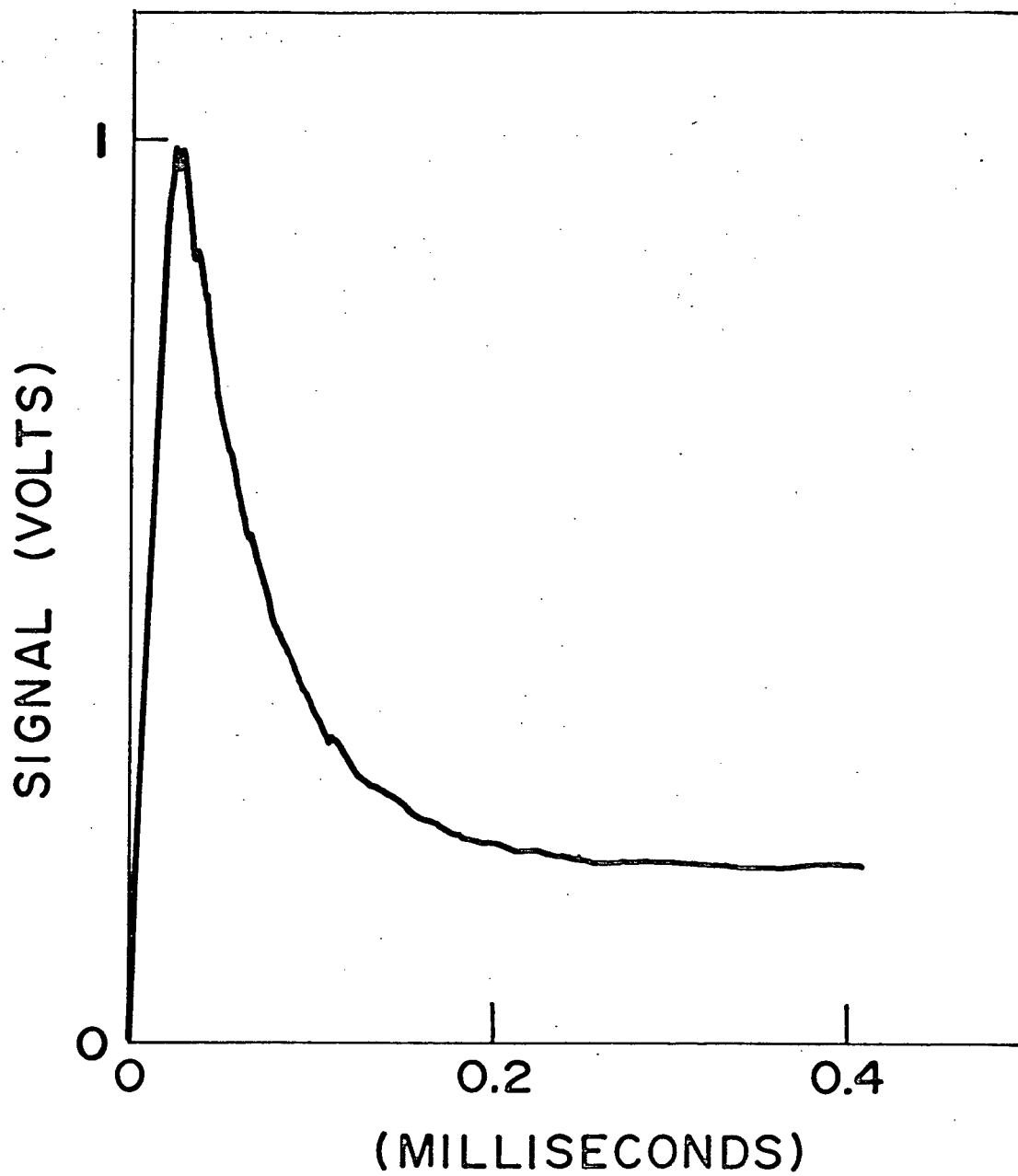10 μsec and the TC parameter was set at 0.1 msec. At the

Figure 7.   Photoelectron Signal Pulse Shape at Terminating
Impedance 100 KΩ

— 59 —

repetition frequency 10 pps of the laser this gave, according
to equations 3.1 and 3.2, a signal-to-noise improvement ratio
of 4.5 and an experimental time constant of 1 second, effect-
ively averaging over ten laser pulses. The magnitude of the
processed signal was maximized by introducing a delay of
approximately 3 μsec between the beginning of the input pulse
and the opening of the boxcar aperture.

Vibrational analysis of the spectrum required the ex-
perimental measurement of the energy separation of the photo-
ionization bands. To facilitate this measurement, a portion
of the laser light was passed through a Fabry-Perot inter-
ferometer, yielding, as the laser scanned, optical fringes
of essentially constant energy separation which were recorded
simultaneously with the photoelectron signal on a two-channel
chart recorder. A sample of the data is presented in Figure
12. The instruments used to record the Fabry-Perot fringes
were photomultiplier EMI 6256S and boxcar integrator CW-1.
Since the output of the Fabry-Perot interferometer was weak,
a relatively high cathode voltage, -800V, was required on the
photomultiplier. The aim in the processing of the Fabry-
Perot signal with the boxcar integrator was good resolution
of the fringes rather than a large signal-to-noise improvement
ratio. Thus the TC parameter was set at its lowest possible
value, 0.1 msec, on boxcar integrator CW-1. The half-width
of the signal pulse from the photomultiplier was 6.8 μsec at

a terminating impedance of 10 KΩ, and the aperture width of
the boxcar integrator was set at 10 μsec. The magnitude of
the output signal was maximized by delaying the boxcar aper-
ture approximately 0.8 μsec from the beginning of the input
pulse. The quoted settings of boxcar integrator CW-1 pro-
duced an experimental time constant of 1 second and a
signal-to-noise improvement ratio of 4.5. The scanning rate
of the laser was such that the period of the fringes was
about 24 seconds. In the recording of the Fabry-Perot fringes,
the boxcar sensitivity and chart recorder sensitivity were
each 5 volts FSD, giving a fringe amplitude between 10% and
20% of the full chart scale (Figure 12). In this application,
the potential difference across the electrodes of the Iodine
cell was set very high (-400 V), just below the arc threshold
at 20°C. This action was taken to increase the visibility of
the weaker bands. The inevitable saturation of the strongest
bands under these conditions was unimportant in this applic-
ation, as the positions of the bands, rather than their amp-
litude, was the item of be measured. The chart recorder
sensitivity on the channel on which the photoionization signal
was recorded was maintained at 5 volts FSD, while the sensit-
ivity of boxcar integrator PAR 160 was varied between 1 volt
and 100 mvolt FSD during a complete scan in order to magnify
the weaker photoionization bands.

The data necessary for a determination of the band

intensities required, along with the photoionization signal,
the simultaneous monitoring of the laser intensity. The
Fabry-Perot interferometer was removed so that the direct
reflected laser light could be recorded. The recording
instruments used were photomultiplier EMI 6256S at a cathode
voltage -600 V followed by boxcar integrator PAR CW-1. In
this application the signal-to-noise characteristics were of
prime importance. Since the laser intensity is a slowly
varying function of wavelength (Figures 10 and 11), resolution
could be sacrificed to achieve excellent signal-to-noise
characteristics. The boxcar settings were TC = 1 msec and
gate width 10 µsec so that at the pulse repetition frequency
of 10 pps, the signal-to-noise improvement ratio was 14 and
the experimental time constant was 10 seconds (equations 3.1
and 3.2), effectively averaging over 100 laser pulses. The
processed signal was maximized by delaying the sampling gate
0.8 µsec from the beginning of the input pulse. On all scans
taken the sensitivity of the boxcar was 0.5 volt FSD and of
the chart recorder, 1 volt FSD. In the recording of the
photoionization signal, the electrode voltage was varied
between -200 and -400 V, and the sensitivities of the record-
ing instruments were constant throughout at 100 mV FSD
(boxcar) and 5 volts FSD (chart recorder), in this application.

Photoionization data were also produced for heated
Iodine vapor. The laser intensity was recorded simultaneously

as described above. Theoretically, a very high vapor temperature is desirable in order to create significant change in the population of the upper vibrational states of the ground electronic state of the molecule. As the vapor increases in density, however, recombination processes decrease the signal intensity, so that very high temperatures are not practical. The lower compartment of the oven which housed the I_2 chamber was held at a temperature in the vicinity of $90^\circ C$, which produced a temperature of about $100^\circ C$ in the upper compartment. This required an applied voltage of 120 volts dc; the oven drew 0.69 amp of current through the heating unit of impedance 173Ω. The saturated vapor pressure within the cell was raised to almost 27 mm Hg, governed by the lowest temperature in the oven, compared with 0.2 mm at room temperature (Gerry and Gillespie, 1932), and the photoionization signal was considerably weakened. The overall sensitivity of the recording instruments was increased over that used in experiments performed at $20^\circ C$. Electrode voltages up to -430 V were possible without electrical saturation. Figure 8 illustrates that the band contour did not change with electrode voltage, as indicated for the (2-0) band at three voltages between -150 and -430 V. The voltage dependence of the peak signal intensity is exponential as illustrated in Figure 9. The sensitivities throughout of the boxcar integrator PAR 160 and chart recorder were 100 mvolt and 1 volt FSD respectively (all bands on scale at -340 V).
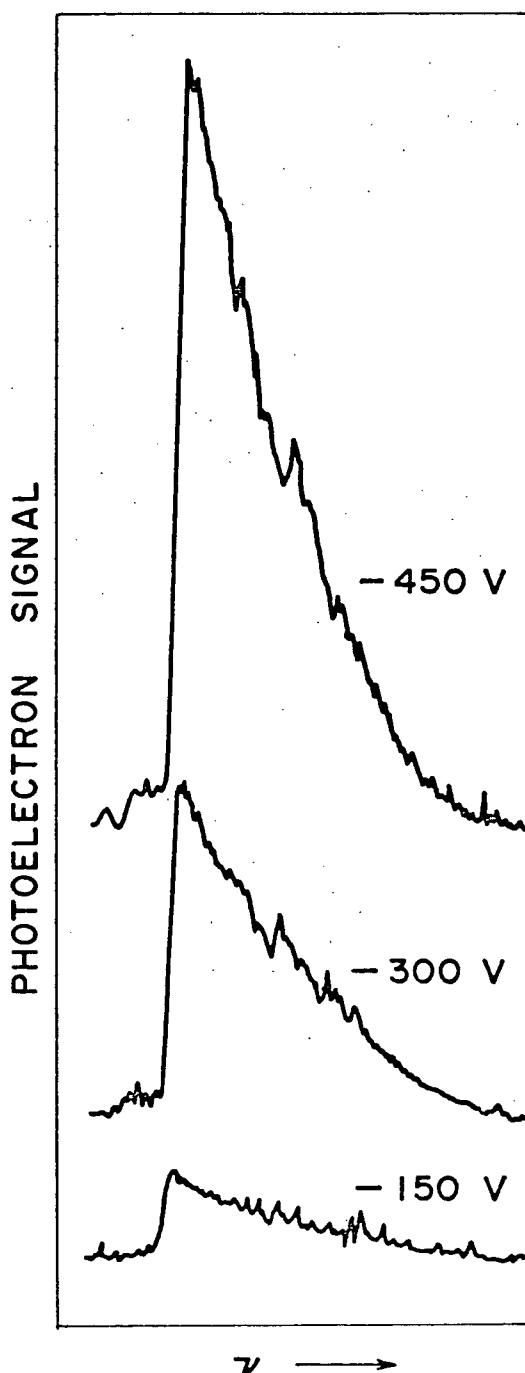
Figure 8.   Voltage Dependence of the Iodine Band Contour
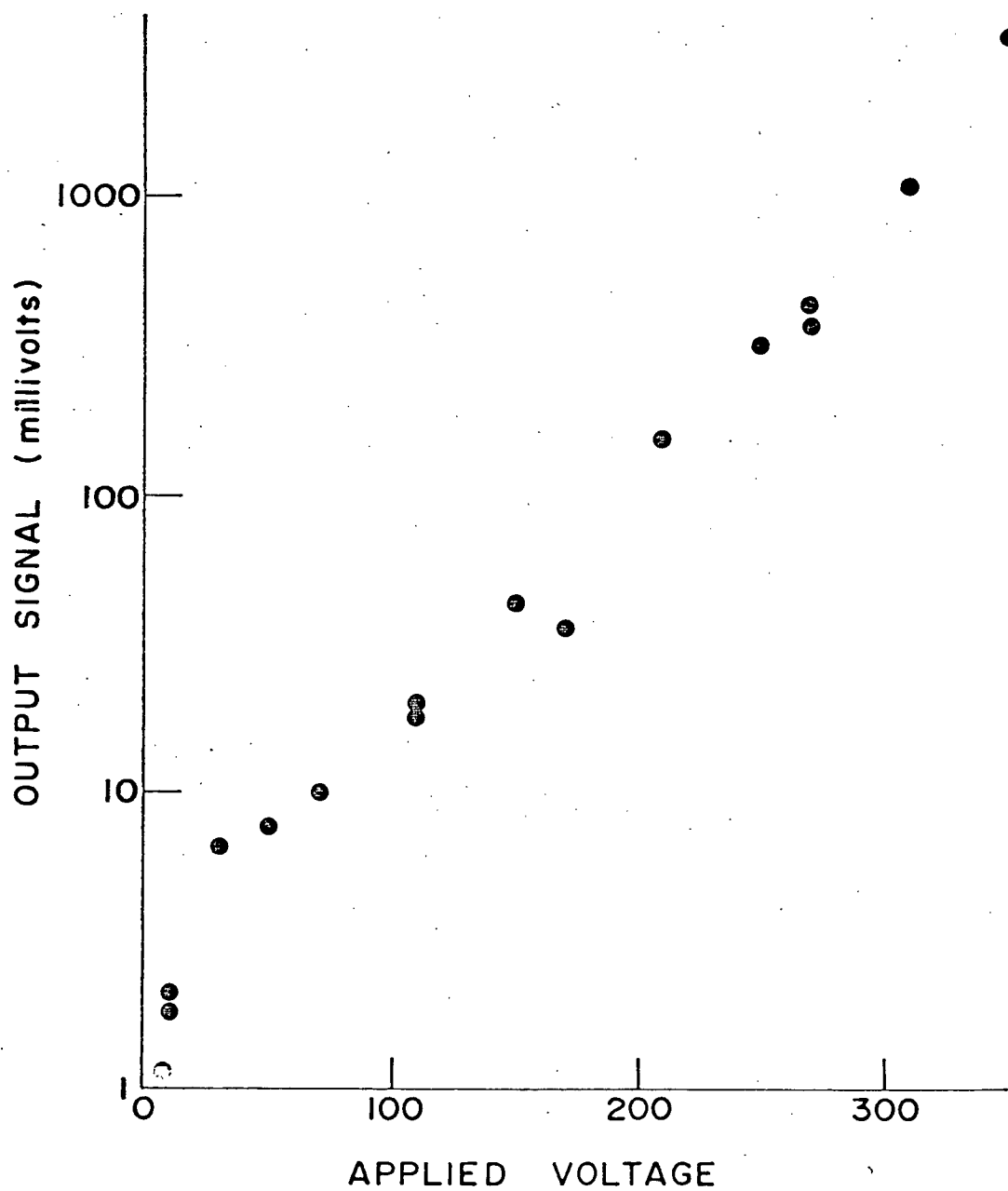Illustrated for a Typical Band at 100°C

Figure 9.   Voltage-Dependence of the Peak Signal
Intensity

4. DATA ANALYSIS

4.1 Introduction

Strong resonant signals were found as the laser frequency was scanned. The off-resonant voltage was negligible. The spectrum consists of a series of approximately equally spaced violet-degraded bands. A typical spectrum at $20^{\circ}C$ is presented in Figure 10, and a typical hot scan ($\simeq 100^{\circ}C$) in Figure 11, accompanied by the laser output. No bands were found to the red of $3800\overset{o}{A}$ in spite of the considerably greater laser power in this region. A part of the spectrum is shown at higher resolution in Figure 12. The number of ions produced at the peak of the stronger bands is on the order of 10^{12} per pulse at -350 V.

The approximately cubic laser power-signal relation (section 4.2) together with the fact that single and double photons were energetically unable to ionize the I_2 molecules, plus the assurance that no resonances can occur for one-photon absorption from the ground state (section 2.5), make it reasonable to assign the observed resonance signal as two photon resonance from the vibrational level v'' of the X 0_g^+ ground state to a vibrational level v' of an intermediate state of symmetry g followed by a nonresonant transition to an ionized state. After some trial and error to ascribe the peaks, one quickly arrives at the assignment of the transitions as presented in Figures 10, 11, and 12. Detailed vibrational
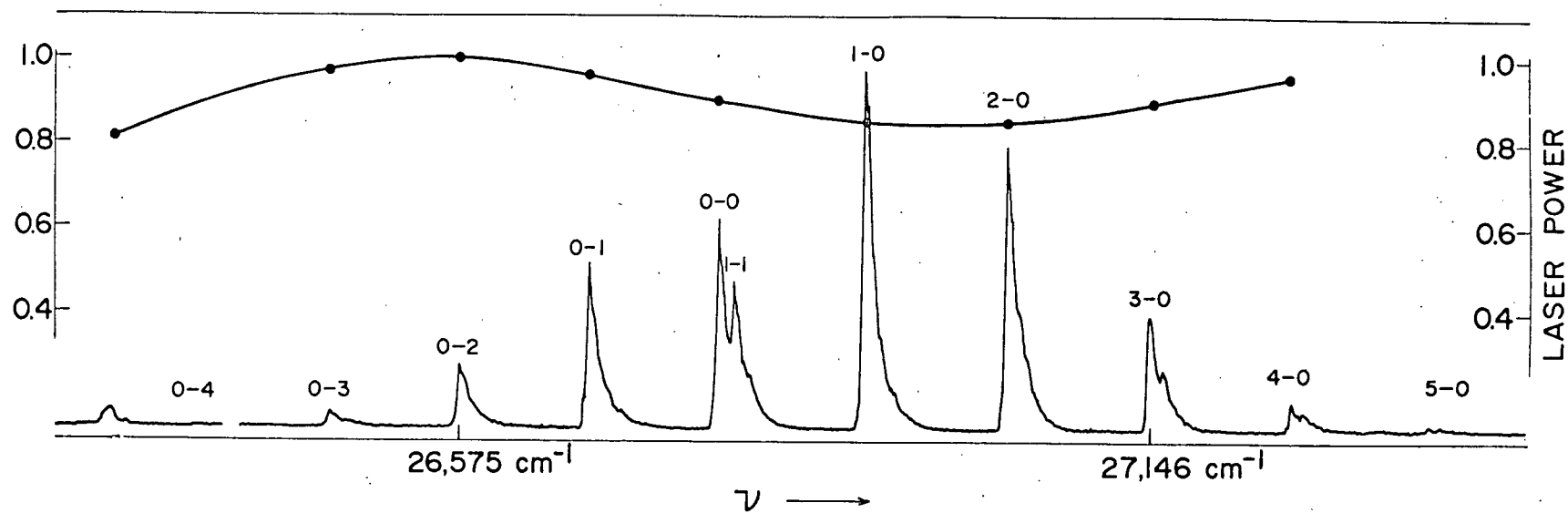
Figure 10.　Typical Photoelectron Spectrum of Iodine
Vapor at 20°C Accompanied by
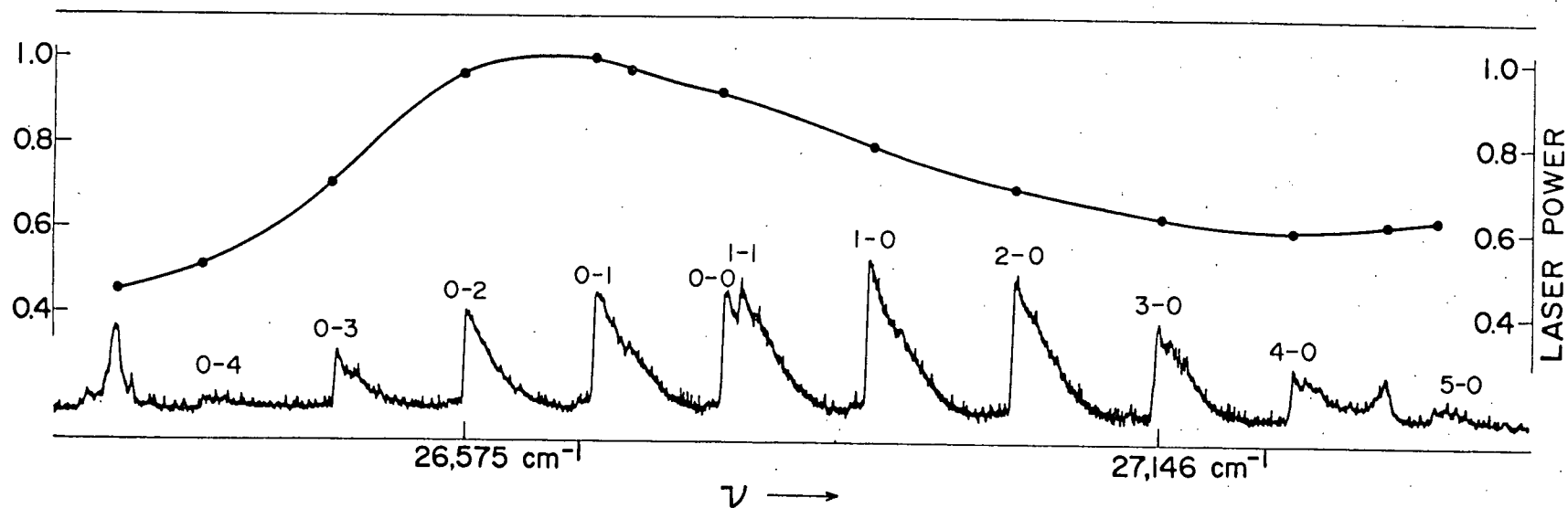Laser Output

Figure 11.   Typical Photoelectron Spectrum of Iodine
Vapor at 100°C Accompanied by
Laser Output
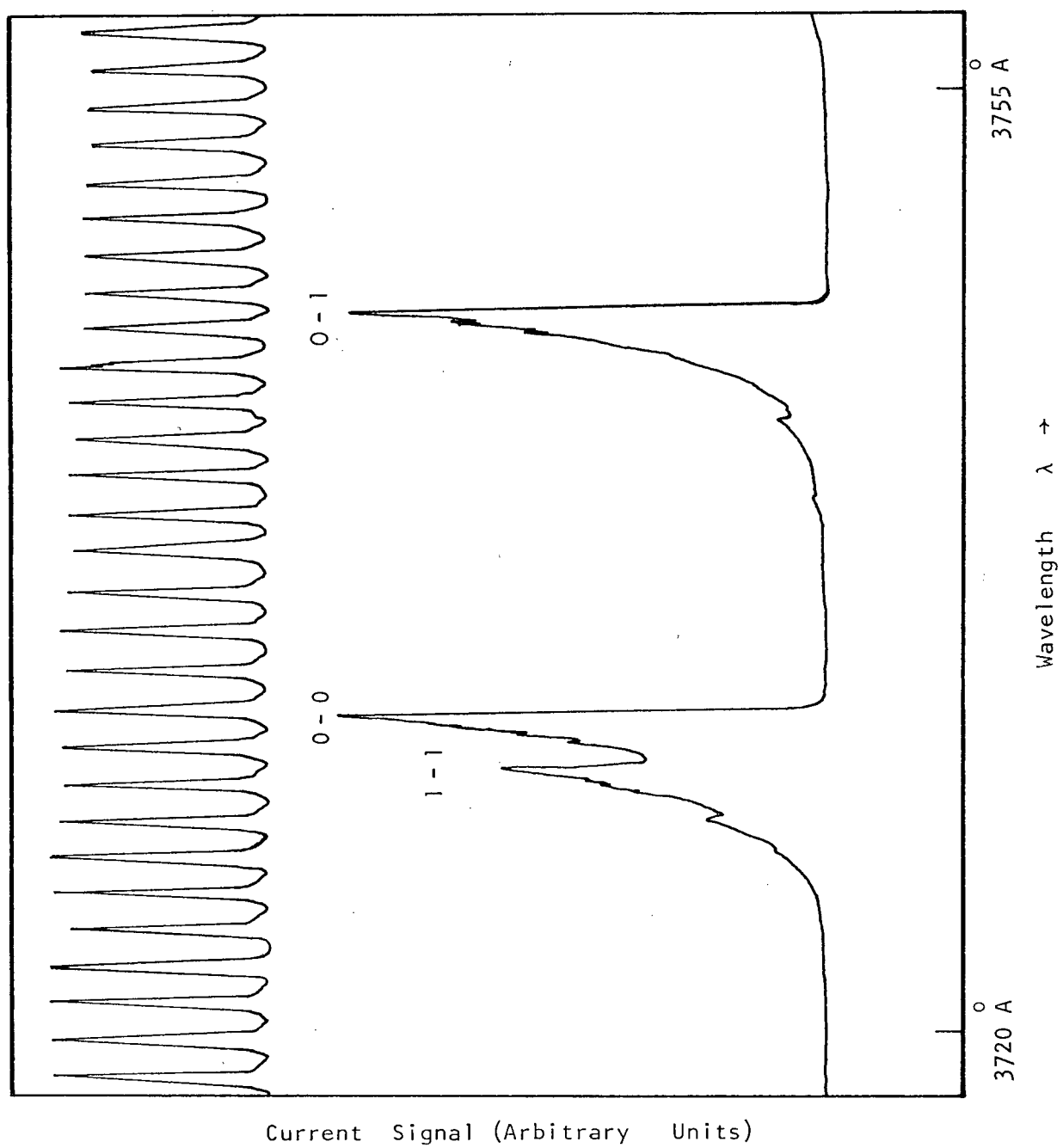
Figure 12.   Portion of the Photoelectron Spectrum at Higher Resolution
              Accompanied by Fabry-Perot Fringes

and rotational analysis of the band system is carried out, and the possible electronic configurations of the new state are explored. The effect of impurities in the sample is discussed briefly.

4.2 Power-Dependence of the Photoionization Signal

As single- and double-photon excitation are energetically unable to ionize the I_2 molecules (section 2.6), any observed resonance signal must be the result of excitation by three or more photons. The power-dependence $I_0{}^N$ of the photoionization signal, upon the intensity I_0 of the incident light, was measured experimentally at the peaks of several bands. The bands chosen were those of the $(v' - 0)$ progressions from (0-0) to (4-0) inclusive, plus the (1-1) band. This choice allowed investigation of the power dependence over a range of (unattenuated) signal strengths. The magnitude of the output signal was determined as the laser intensity was varied with up to four calibrated neutral density filters. The filters, which were identical, each have a density $K(\lambda)$ as noted in Table II. The power dependence N may be determined from the slope of a plot of the log of the photoionization signal intensity versus the number of filters attenuating the laser beam (section 2.1). The relationship is (equation 2.2):

$$N = - \frac{slope}{K(\lambda)} \quad .$$

A sample plot is given (Figure 13) for the (1-0) band.
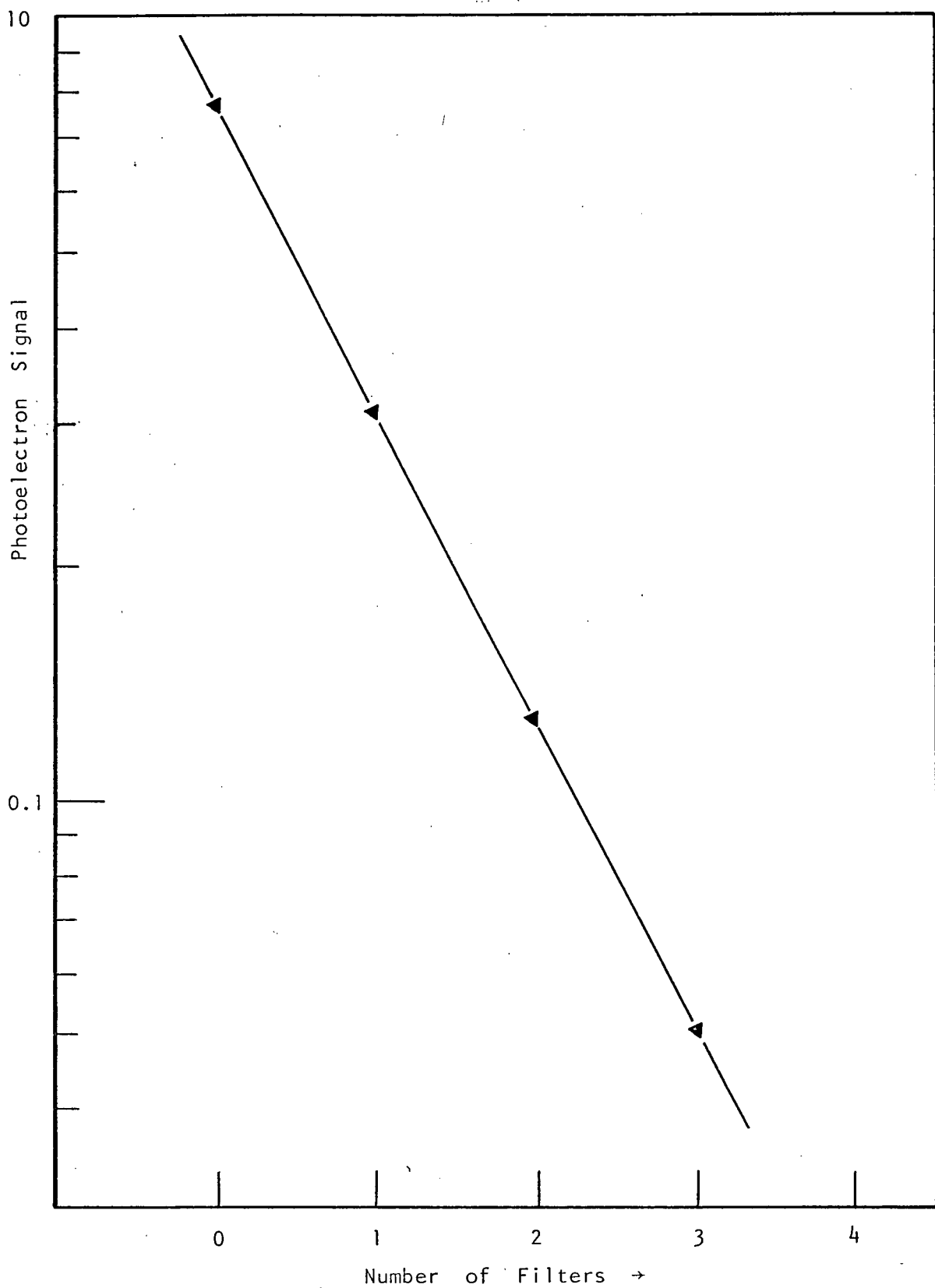
Figure 13.   Dependence of Signal Intensity on Laser Power Illustrated
for the (1-0) Band.

Band	λ_{LASER} (Å)	Filter Density $K(\lambda)$	Power Dependence $N= -slope/K(\lambda)$
(0-0)	3733.10	0.164	2.34
(1-1)	3731.18	0.164	2.50
(1-0)	3716.44	0.166	2.23
(2-0)	3699.98	0.167	2.31
(3-0)	3683.76	0.168	2.69
(4-0)	3667.78	0.169	2.75

Table II. Power-Dependence of the Photoionization Signal

The power-dependence of the chosen bands varies from $I_0^{2.23}$ to $I_0^{2.75}$ (Table II). In general, the stronger the band, the lesser is the power-dependence measured. As the electric signal may not be perfectly linearly related to the tripling process because of possible saturation and avalanche breakdown, the results are consistent with the expected I_0^3 relation.

4.3 Vibrational Analysis

The vibrational constants ω_e' and $\omega_e x_e'$, plus the minimum energy T_e of the electronic potential well may be determined for the upper (resonant) electronic state of I_2 by measuring the separation of the heads of the photoionization bands, as described in section 2.6. Measurements of the spacing of the photoionization band heads, in units corresponding to the number of Fabry-Perot fringes, were taken from three different charts each of which recorded the laser light, passed through a Fabry-Perot interferometer, simultaneously with the I_2 photoionization signal. The measurements from the three charts are tabulated in Table III for the $(0-v'')$ and $(v'-0)$ bands, and are tabulated in Table VII for the $(1-v'')$ and $(v'-1)$ bands of I_2. Each of the $(v'-1)$ bands is resolved from the accompanying $(v'-0)$ band, while the bands of the $(1-v'')$ progression are only occasionally distinct. Hence Table VII contains only selected entries. Since the wavelength tuning system of the dye laser was pushed beyond

its quoted performance limit (section 3.2), the operation of this system was at some points slightly erratic. This effect was the main source of uncertainty in the measurement of the separation of the bands. The magnitude of the uncertainty in the measurements presented in Tables III and VII is better than 1% of the distance between two adjacent bands.

The Fabry-Perot interferometer may be calibrated by comparing the spacing of the $(0-v'')$ bands with the well-known vibrational levels of the ground electronic state of I_2 which are described in section 2.6 and listed in Table I. Once the calibration of the fringes is complete, the separation of the $(v'-0)$ and $(v'-1)$ bands may be converted to wavenumber units, and the vibrational constants calculated for the upper electronic state. The Fabry-Perot interferometer was calibrated using four pairs of bands, from (0-0) to (0-4) inclusive. The calculations are presented in Table IV and yield an average calibration of 9.961 ± 0.034 cm^{-1} per fringe. Applying this calibration factor, the separation in wavenumber units of the $(0-v'')$ and $(v'-0)$ photoionization bands of I_2, averaged over three charts, is given in Table V. Similarily, Table VIII contains the separation of the $(1-v'')$ and $(v'-1)$ bands in wavenumber units.

Calculation of the vibrational constants ω_e' and $\omega_e x_e'$ was carried out separately with the $(v'-0)$ progression and the $(v'-1)$ progression of I_2. Consider first the $(v'-0)$ bands.

Table V contains the second-differences in the vibrational energy which, according to equation 2.5, are in a first approximation equal to $2\omega_e x_e'$. The average of these measured second differences is 1.195 cm^{-1}, and thus the experimentally determined value of the anharmonic vibrational constant $\omega_e x_e'$ is 0.06 cm^{-1} for the upper electronic state of I_2. This vibrational constant was then used in the calculation of the harmonic vibrational constant ω_e' as follows. Keeping only the first two terms of equation 2.4, the first-differences in the experimental vibrational energy may be expressed:

$$\Delta G_E = \omega_e' - \omega_e x_e' (2v' + 2)$$

where v' is the quantum number of the lower vibrational state involved in the comparison. Thus,

$$\omega_e' = \Delta G_E + \omega_e x_e' (2v' + 2).$$

Using the experimental value $\omega_e x_e' = 0.060$ cm^{-1}, several calculations of ω_e' are presented in Table VI for bands of the (v'-0) progression. The average of the values determined for ω_e' of the upper electronic state is 241.45 cm^{-1}.

Vibrational analysis carried out on bands of the (v'-1) progression was more complex, since the (2-1) band is not resolved from (1-0) and its position cannot be measured. Calculation of the anharmonic vibrational constant $\omega_e x_e'$ proceeded as follows. From data in Table VII, the fringe separation of the (1-1) and (3-1) bands is 47.894 fringes for a double-quantum transition. Thus, using the notation of

Table VIII, we have:

$$2x + 2y = 47.894 \ . \tag{4.1}$$

We also know the following second differences from Table VIII:

$$9.961(2x - 2y) = 2\omega_e x_e' \ , \tag{4.2}$$

$$9.961 \ (2y) - 237.19 = 2\omega_e x_e' \ , \tag{4.3}$$

where $\omega_e x_e'$ must be in wavenumber units. The set of three equations in three unknowns, 4.1, 4.2 and 4.3, may easily be solved by substitution. The only unknown of value is $2\omega_e x_e'$, for which the solution is 0.897 cm^{-1}. One other evaluation of the second difference $2\omega_e x_e'$ is available directly from the data of Table VIII, using the (3-1), (4-1) and (5-1) bands. This value is 2.13 cm^{-1}. Thus the average value of $\omega_e x_e'$ obtained from the bands of the $(v'-1)$ progression is 0.76 cm^{-1}. Table IX contains the calculations leading to a determination of the harmonic vibrational constant ω_e', similar to the analysis of the $(v'-0)$ bands. Two evaluations of ω_e' are available directly from the table, while a third may be obtained as follows. The expressions:

$$9.961(2x) + 3.04 = \omega_e' \ , \tag{4.4}$$

$$9.961(2y) + 4.56 = \omega_e' \tag{4.5}$$

from Table VIII plus equation 4.1:

$$2x + 2y = 47.894$$

give three equations in three unknowns which, when solved by substitution for ω_e', yield the value 242.33 cm^{-1}. The average of the experimentally determined values of ω_e' is

then 242.76 cm^{-1}.

The vibrational analysis carried out separately with the (v'-0) and (v'-1) progressions agrees very well: ω_e' = 241.45 cm^{-1} ± 1% versus 242.76 cm^{-1} ± 1% and $\omega_e x_e'$ = 0.60 cm^{-1} versus 0.76 cm^{-1} respectively. These evaluations of the vibrational constants ω_e' and $\omega_e x_e'$ relied upon a simple averaging procedure. The comparison of measured transition energies with calculated energies is given greater internal consistency, however, by applying a least-squares fit of the observations to a quadratic function:

$$E(v') = T_e + \omega_e'(v' + \tfrac{1}{2}) - \omega_e x_e'(v' + \tfrac{1}{2})^2$$

with each observation given equal statistical weight (Pryce, 1976). In order to determine the absolute positions of the resonances observed in I_2, the wavelength output of the dye laser must be established. The energy of the (0-0) transition was placed at 53,576.00 ± 1 cm^{-1} by Dalby and Tai (1976) using a 3-meter Ebert spectrometer plus a nickel arc reference spectrum. The large error arises from the fact that the position at which the laser calibration was done relative to the peaks in the I_2 resonance spectrum was not well-defined. The least-squares analysis of Pryce (1976) gives the results:

$$E(v') = 53,562.75 \pm 0.35 + (241.4 \pm 0.4)(v' + \tfrac{1}{2})$$
$$- (0.58 \pm 0.06)(v' + \tfrac{1}{2})^2 \quad cm^{-1}.$$

The errors quoted are relative errors. Since the absolute

Band	Separation of Successive Band Heads				
	Chart A	Reverse Scan on A (Number of Fabry-Perot Fringes)	Chart B	Chart C	Average
(0-4)					
	10.553			*	10.553
(0-3)					
	10.577			*	10.577
(0-2)					
	10.705			10.614	10.660
(0-1)					
	10.600			10.743	10.672
(0-0)					
	12.212		11.931	11.986	12.043
(1-0)					
	11.847		12.175	12.071	12.031
(2-0)					
	12.047		11.841	11.914	11.934
(3-0)					
	11.824	11.918	11.883	11.915	11.885
(4-0)					
	11.759	11.588	12.063		11.803
(5-0)					

* Bands not distinct.
  Bands not marked were not included in the scan.

Table III. Fringe Separation of the $(0-v'')$ and $(v'-0)$ Bands of I_2

Band	Separation in Number (n) of Fabry-Perot Fringes (Table III)	True Fringe Spacing (2n) of Vibrational Levels	ΔG (cm^{-1}) (Table I)	Calibration of Fringes $= \Delta G/2n$ $(cm^{-1}$ per fringe)
(0-0)				
	10.672	21.344	213.34	9.995
(0-1)				
	10.660	21.320	212.11	9.949
(0-2)				
	10.577	21.154	210.87	9.968
(0-3)				
	10.553	21.106	209.63	9.932
(0-4)				

Mean = 9.961 ± 0.034 cm^{-1} per fringe

Table IV.   Calibration of the Fabry-Perot Interferometer.

Band	Separation in Number (n) of Fabry-Perot Fringes (Table IV)	Fringe Separation of Bands for Double-Quantum Transition (2n)	Experimental Energy Separation ΔG_E (cm^{-1})	Second Difference $\Delta^2 G_E \simeq 2\omega_e x_e'$ (cm^{-1})
(0-4)				
	10.553	21.106	210.24	
(0-3)				
	10.577	21.154	210.71	
(0-2)				
	10.660	21.320	212.37	
(0-1)				
	10.672	21.344	212.61	
(0-0)				
	12.043	24.086	239.92	
(1-0)				0.24
	12.031	24.062	239.68	
(2-0)				1.94
	11.934	23.868	237.74	
(3-0)				0.96
	11.885	23.770	236.78	
(4-0)				1.64
	11.803	23.606	235.14	
(5-0)				

Table V.   Energy Separation of the (0-v") and (v'-0) Bands of I$_2$.

Band	ΔG_E (Table V)	$\chi = 0.60(2v'+2)$	Experimental Evaluation of ω_e' ($\Delta G_E + \chi$)
	(cm^{-1})	(cm^{-1})	(cm^{-1})
(0-0)			
	239.92	1.20	241.12
(1-0)			
	239.68	2.40	242.08
(2-0)			
	237.74	3.60	241.34
(3-0)			
	236.78	4.80	241.58
(4-0)			
	235.14	6.00	241.14
(5-0)			

Table VI. Experimental Evaluation of ω_e' Using the (v'-0) Progression

Band	Separation of Band Heads from (0-0)				
	Chart A	Reverse Scan on A (Number of Fabry-Perot Fringes)	Chart B	Chart C	Average
(1-5)	*				
(1-4)	-30.435				-30.435
(1-3)	*				
(1-2)	*				
(1-1)	1.412		1.436	1.300	1.383
(2-1)	**		*	*	
(3-1)	25.389		*	25.271	25.330
(4-1)	37.224	37.365	37.213	37.143	37.236
(5-1)	49.024	49.118	49.042	48.957	49.035

*Band not distinct.

Bands not marked were not included in the scan.

**Fabry-Perot fringes erratic.

Table VII.   Fringe Separation of the (1-v") and (v'-1)

Bands of I_2.

Band	Separation in Number (n) of Fabry-Perot Fringes (Table VII)	Fringe Separation of Bands for Double-Quantum Transition (2n)	Experimental Energy Separation ΔG_E (cm^{-1})	Second Difference $\Delta^2 G_E \simeq 2\omega_e x_e'$ (cm^{-1})
(1-4)				
	31.818	63.636	638.88	
(1-1)				
	x	2x	9.961(2x)	
(2-1)				$2\omega_e x_e'$
	y	2y	9.961(2y)	
(3-1)				$2\omega_e x_e'$
	11.906	23.812	237.19	
(4-1)				2.13
	11.799	23.598	235.06	
(5-1)				

Table VIII. Energy Separation of the $(1-v'')$ and $(v'-1)$ Bands of I_2.

Band	ΔG_E (Table VIII) (cm^{-1})	$\chi = 0.76(2v'+2)$ (cm^{-1})	Experimental Evaluation of ω_e' $(\Delta G_E + \chi)$ (cm^{-1})
(1-1)			
	9.961(2x)	3.04	9.961(2x)+3.04
(2-1)			
	9.961(2y)	4.56	9.961(2y)+4.56
(3-1)			
	237.19	6.08	243.28
(4-1)			
	235.06	7.60	242.66
(5-1)			

Table IX. Experimental Evaluation of ω_e'
         Using the (v'-1) Progression.

Band	Transition Energy $1/\lambda$ in vacuum (cm^{-1})		
	Observed	Calculated	Δ
(0-4)	52,730.08	52,730.22	-0.14
(1-5)	-	52,762.07	-
(0-3)	52,940.32	52,939.85	0.47
(1-4)	52,969.68	52,970.46	-0.78
(0-2)	53,151.04	53,150.72	0.32
(1-3)	-	53,179.09	-
(0-1)	53,363.40	53,362.83	0.57
(1-2)	-	53,390.96	-
(0-0)	53,576.00	53,576.17	-0.17
(1-1)	53,603.56	53,603.07	0.49
(1-0)	53,815.92	53,816.41	-0.49
(2-1)	-	53,842.15	-
(2-0)	54,055.60	54,055.49	0.11
(3-1)	54,080.62	54,080.07	0.55
(3-0)	54,293.34	54,293.41	-0.07
(4-1)	54,317.82	54,316.83	0.99
(4-0)	54,530.12	54,530.17	-0.05
(5-1)	54,552.88	54,552.43	0.45
(5-0)	54,765.26	54,765.77	-0.51
(6-1)	-	54,786.87	-

Table X. Energies of the Observed Resonances in I_2.

position was established much less accurately than the band

separations, the absolute error in $\bar{T}_e$ is at least 1 cm^{-1}.

Table X lists the positions of the observed resonances in

I_2, in which the band separations of Table V and VIII have

been added or subtracted, as applicable, to the one absolute

reference energy available, that of the (0-0) transition.

The agreement of observed and calculated transition energies

is excellent (Table X).

4.4 Rotational Analysis

Some qualitative conclusions regarding the rotational

constants of the molecule may be drawn from the appearance

of the photoionization bands. The degrading of the bands

to the violet indicates that $B_v' > B_v''$ (section 2.5). The

decrease in the slope of the bands as the temperature of the

vapor increases confirms that $B_v' > B_v''$. Furthermore, the

narrowness of the bands indicates that the rotational energy

levels are very closely spaced (equations 2.8 to 2.12) and

it is expected that B_v' is only slightly larger than B_v''.

The separation of the Iodine nucleii in the upper (resonant)

electronic states is thus slightly smaller than 2.666Å, the

separation in the ground electronic state. Detailed rota-

tional analysis is done by the Frank-Condon method.

The intensity $S_{v',v''}$ of a vibrational transition in

the triple-photon ionization spectrum of I_2 depends upon the

population of the initial level, the Frank-Condon factor

between the vibrational states, the laser intensity to a power N, and the photoionization efficiency $P(v',\nu)$ which is an unknown function of the upper-vibrational-state quantum number and of the molecule's total energy prior to ionization. We may write:

$$S_{v',v''} = K \left\langle \psi_{v'} | \psi_{v''} \right\rangle^2 I_0^{2.7} P(v',\nu) e^{-G_0(v'')hc/kT} .$$

Since the laser intensity is a slowly varying function of wavelength (Figures 10 and 11), the assignment of the power-dependence N is not critical. The power-dependence adopted is an average value 2.7 for all the bands, representing conditions in which there is a minimum of optical or electrical saturation in the photoionization process. The conversion of $S_{v',v''}$ to absolute intensity is contained in the constant K which includes the effect of the experimental parameters which influence intensity, such as electrode voltage and the current amplification within the Iodine cell.

The relative band intensities were measured experimentally at Iodine vapor temperatures $20^\circ C$ and $100^\circ C$. Note that the population of the higher vibrational levels in the ground electronic state of I_2 increases measurably (Table XI) over this temperature range. Two sets of intensity measurements were obtained at $100^\circ C$, at electrode voltages -300 V and -430 V; these were analyzed individually since most of the bands were visible at low electrode voltages. At room temperature, the bands differed much more in magnitude than at

v"	Vibrational Energy $G(v")-G(0)$ (cm^{-1})	Relative Population $e^{-[G(v")-G(0)]/kT}$	Fraction of Total Sample (%)
I. VAPOR TEMPERATURE 20°C			
0	0	1	64.9
1	213.34	0.351	22.8
2	425.45	0.124	8.05
3	636.32	0.0441	2.86
4	845.95	0.0158	1.03
5	1054.34	0.00567	0.37
6	1261.47	0.00205	0.13
		Partition Function = 1.54	
II. VAPOR TEMPERATURE 100°C			
0	0	1	56.2
1	213.34	0.439	24.7
2	425.45	0.194	10.9
3	636.32	0.0860	4.83
4	845.95	0.0384	2.16
5	1054.34	0.0172	0.97
6	1261.47	0.00773	0.43
		Partition Function = 1.78	

Table XI.   Relative Equilibrium Population of Vibrational States in the Ground Electronic State of I_2.

higher temperatures, and it was necessary to combine the
intensity measurements from several scans obtained at dif-
ferent electrode voltages. The relative intensities of the
strongest photoionization bands were determined from data
obtained with minimum electrical saturation at the low elec-
trode voltage -200 V. In addition, scans taken at the inter-
mediate electrode voltage -240 V and the maximum voltage
-400 V, putting the strong bands off-scale in both cases,
provided data for calculation of the relative intensities of
the remaining bands.

The strength of a vibrational transition is divided
among the various accompanying rotational transitions. When
a band is unresolved, the strength of the vibrational
transition is therefore determined from the area under the
band. In the I_2 photoionization spectrum, however, it
sufficed to measure the amplitude of the band heads, as the
bands all had a similar shape at a given vapor temperature
and in the absence of saturation. The dependence of the band
amplitudes upon the laser power and upon the population of the
initial vibrational level was removed to arrive at experimental
values $\hat{S}_{v',v''} \propto \langle \psi_{v'} | \psi_{v''} \rangle^2 P(v',v)$. The photoionization
efficiency $P(v',v)$ is not well established for molecules.
However, the effects of this parameter were not expected
to be large for the majority of the bands, and $P(v',v)$ was
initially assumed constant. The absolute intensities were

not required in the rotational analysis. Rather, normalization
was carried out, for each set of data, by summing the contrib-
utions from a single progression and dividing all band amp-
litudes in the chosen set by this value, so that $\sum_{v'} \hat{S}_{v',v''} = 1$
and $\sum_{v''} \hat{S}_{v',v''} = 1$. This resulted in experimental band inten-
sities which are directly comparable with the theoretical
Franck-Condon factors, for which $\sum_{v'} \langle \psi_{v'} | \psi_{v''} \rangle^2 = 1$ and
$\sum_{v''} \langle \psi_{v'} | \psi_{v''} \rangle^2 = 1$. The results are presented in Table XII.

Table XIII contains theoretical Franck-Condon factors
calculated in the harmonic approximation according to the
method of section 2.7, for transitions between the ground
($\omega_e'' = 214.57$ cm^{-1}) and two-photon resonant ($\omega_e' = 241.4$ cm^{-1})
electronic states of I_2. It is clear from direct comparison
of the Franck-Condon factors with the experimental band in-
tensities that $|\Delta r|$ (or ∂) lies between 0.075 and 0.125Å. Note,
however, that the transition strengths of certain of the vib-
rational transitions vary rapidly, as a function of ∂, with
respect to one another. Thus, the ratios of certain Franck-
Condon factors provide a much more sensitive comparison with
the experimental data. The four most sensitive ratios are
presented in Table XIV for a narrow range of ∂ (0.096 - 0.104Å).
Comparison of these theoretical ratios with the mean exper-
imental intensity ratios yields four values of ∂ which are in
close agreement. We may conclude that $|\Delta r| = 0.0988$Å $\pm$ 2%.
Thus, the internuclear separation in the resonant electronic

Band	Relative Intensity			
	Bands at 20°C	Bands at 100°C (-300 V)	Bands at 100°C (-430 V)	Mean
(0-0)	0.17	0.11	0.13	0.14
(1-0)	0.39	0.20	0.25	0.28
(2-0)	0.31	0.27	0.28	0.28
(3-0)	0.11	0.23	0.21	0.18
(4-0)	0.022	0.15	0.10	0.090
(5-0)	0.004	0.048	0.027	0.026
(0-1)	0.32	0.19	0.24	0.25
(1-1)	(0.22)	(0.12)	(0.13)	(0.16)
(2-1)				
(3-1)				
(4-1)	(0.071)		(0.12)	(0.093)
(5-1)	(0.024)	(0.11)	(0.080)	(0.070)
(6-1)	(0.006)		(0.051)	(0.029)
(0-2)	0.36	0.40	0.30	0.35
(2-2)		0.15		0.15
(3-2)			(0.17)	(0.17)
(0-3)	0.42	1.23	0.42	0.69
(2-3)		(0.15)	(0.24)	(0.19)
(0-4)	0.26	1.36	0.40	0.68
(1-4)	(0.22)		(0.098)	(0.16)
(1-5)	(0.27)			(0.27)

Bracketed values have uncertainty up to a factor of 2.
All others are assigned an uncertainty of 30%.

Table XII.   Relative Intensities of the Photoionization
             Bands of I_2.

Band	Franck-Condon Factors		
	$\delta = 0.075$ Å	$\delta = 0.100$ Å	$\delta = 0.125$ Å
(0-0)	0.299	0.117	0.035
(1-0)	0.338	0.236	0.111
(2-0)	0.213	0.252	0.180
(3-0)	0.097	0.189	0.204
(4-0)	0.036	0.112	0.178
(5-0)	0.012	0.056	0.129
(0-1)	0.383	0.267	0.125
(1-1)	0.012	0.152	0.193
(2-1)	0.090	0.005	0.109
(3-1)	0.197	0.045	0.013
(4-1)	0.166	0.132	0.011
(5-1)	0.092	0.153	0.070
(0-2)	0.222	0.287	0.214
(2-2)	0.138	0.114	0.000
(3-2)	0.000	0.110	0.073
(0-3)	0.076	0.194	0.236
(2-3)	0.006	0.103	0.087
(0-4)	0.017	0.092	0.188
(1-4)	0.170	0.201	0.041
(1-5)	0.057	0.177	0.135

Table XIII. Theoretical Franck-Condon Factors for Selected Vibrational Transitions Between the Ground and Resonant Electronic States of I_2.

	Theoretical Franck-Condon-Factor Ratios					Mean Experimental Intensity Ratios
	$\partial=0.096$ Å	$\partial=0.098$ Å	$\partial=0.100$ Å	$\partial=0.102$ Å	$\partial=0.104$ Å	
$\dfrac{F(1-1)}{F(0-0)}$	0.943	1.111	1.296	1.500	1.724	1.154
$\dfrac{F(3-0)}{F(0-0)}$	1.279	1.437	1.611	1.803	2.013	1.353
$\dfrac{F(1-1)}{F(1-0)}$	0.509	0.576	0.645	0.718	0.793	0.561
$\dfrac{F(1-1)}{F(0-1)}$	0.450	0.509	0.571	0.635	0.702	0.636

Table XIV.   Comparison of the I_2 Experimental Intensity
Ratios with the Ratios of the Theoretical
Franck-Condon Factors from
∂ = 0.096 to 0.104 Å.

state is $r_e{'} = 2.567 \pm 0.002\overset{o}{A}$. The upper-state rotational con-
stant is $B_e{'} = 0.04029 \pm 0.00007$ cm^{-1}, and $\Delta B/B_e{''} = 0.079 \pm 3\%$.
A plot, as a function of total molecular energy, of the ratios
of the mean experimental band intensities to the corresponding
theoretical Franck-Condon factors at $\partial = 0.099\overset{o}{A}$ (Figure 14),
indicates that the photoionization yield $P(v',v)$ of I_2 is not
constant between 80,050 and 82,250 cm^{-1}. Typical uncertainties
in the experimental values are indicated in the Figure. The
photoionization yield has an apparent resonance in the vicinity
of 80,000 cm^{-1}. Thereafter, there is a slight downward trend
with increasing molecular energy, as observed by Myer and
Samson (1970). Each of six absorption progressions exhibit
independently these two features. The transitions (0-0), (1-1),
(3-0), (1-0) and (0-1), whose intensity ratios were the basis
for determining $|\Delta r|$, have total energy between 80,360 and
81,550 cm^{-1} and thus lie in the plateau region where the
photoionization yield of I_2 is roughly constant.

4.5 Band Contour Analysis

Applying the rotational analysis of the upper electronic
state (section 4.4) to the branch contour formulae of section
2.8, which convolutes the intensity distribution of each rota-
tional branch with the laser spectrum, one may calculate the
contours of the five separate rotational branches O, P, Q, R
and S. Appendix B contains these intermediate calculations.
Knowing the intensity distribution between the branches,

RATIO OF NORMALIZED
INTENSITIES TO THEORETICAL
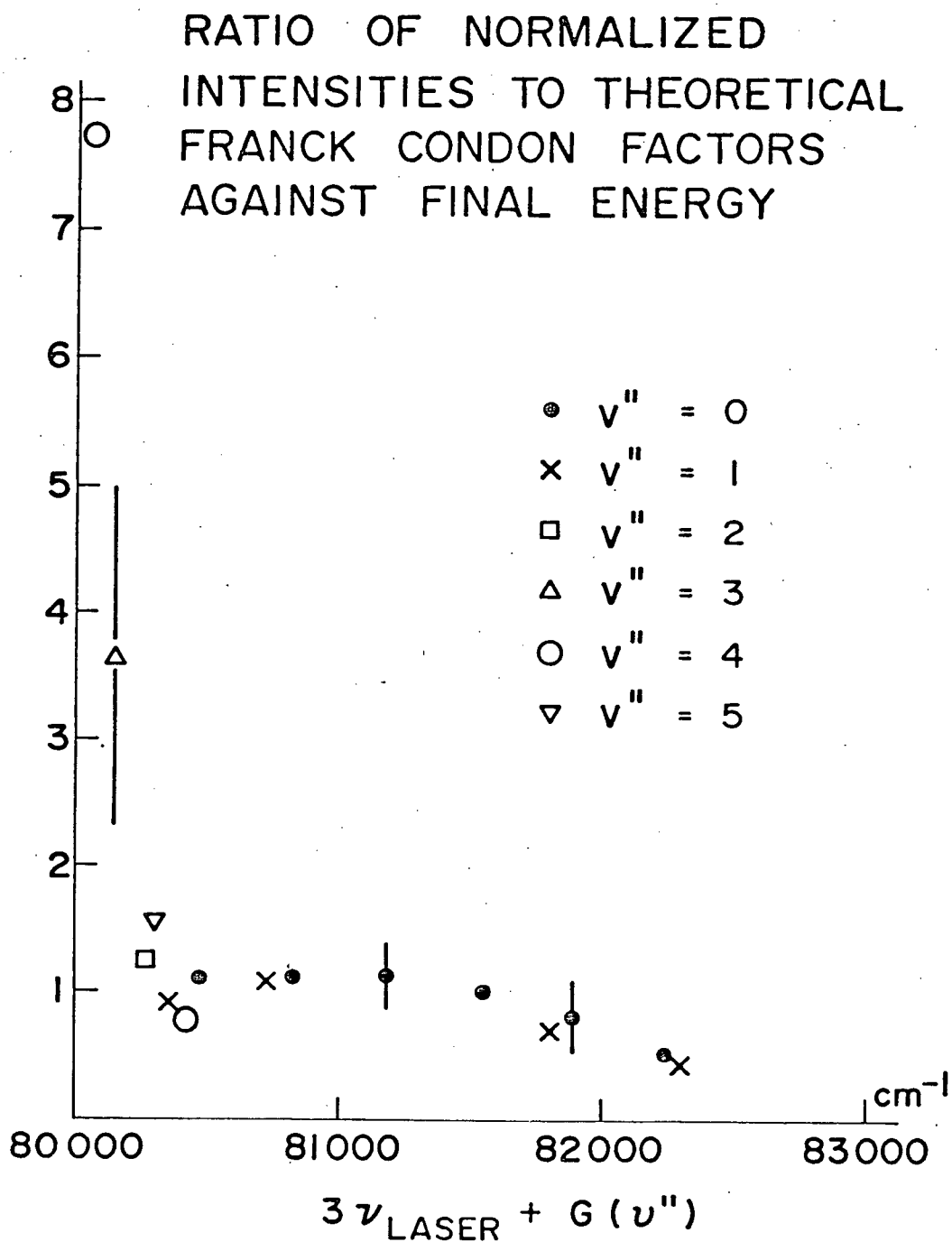FRANCK CONDON FACTORS
AGAINST FINAL ENERGY

Figure 14.

discussed in detail in section 2.8, one may then sum the contributions of all branches to arrive at the band contour applicable to a particular electronic transition.

In two-photon absorption to a resonant state, three electronic transitions are possible: $0_g^+ \rightarrow 0_g^+$, $0_g^+ \rightarrow 1_g$, and $0_g^+ \rightarrow 2_g$ (section 2.4). The contours of the photoionization bands of I_2 predicted for each of the three possible electronic transitions at $20^{\circ}C$ are presented in Figures 15, 16 and 17. The $0_g^+ \rightarrow 0_g^+$ contour varies according to the relative contributions of the 0_u^+ and 1_u intermediate states. The two extreme cases plus an intermediate case are depicted in Figure 15 for this electronic transition. The peak of the band contour for each electronic transition lies very close to the band origin ν_o.

At a resolution of 1.5 cm^{-1}, the theoretical band contours are too similar to indicate decisively the electronic configuration of the resonant state of I_2. However, certain of the transitions are found to be highly improbable. The band contours observed in our numerous experimental spectra have in general a smooth rise to the peak on the steep side, followed by exponential drop-off with a slight hesitation occurring near the peak on this side. It is probable that the $0_g^+ \rightarrow 2_g$ transition may be ruled out since the theoretical band contour shows features of equal prominence on both sides of the peak, contrary to observation. It is also evident
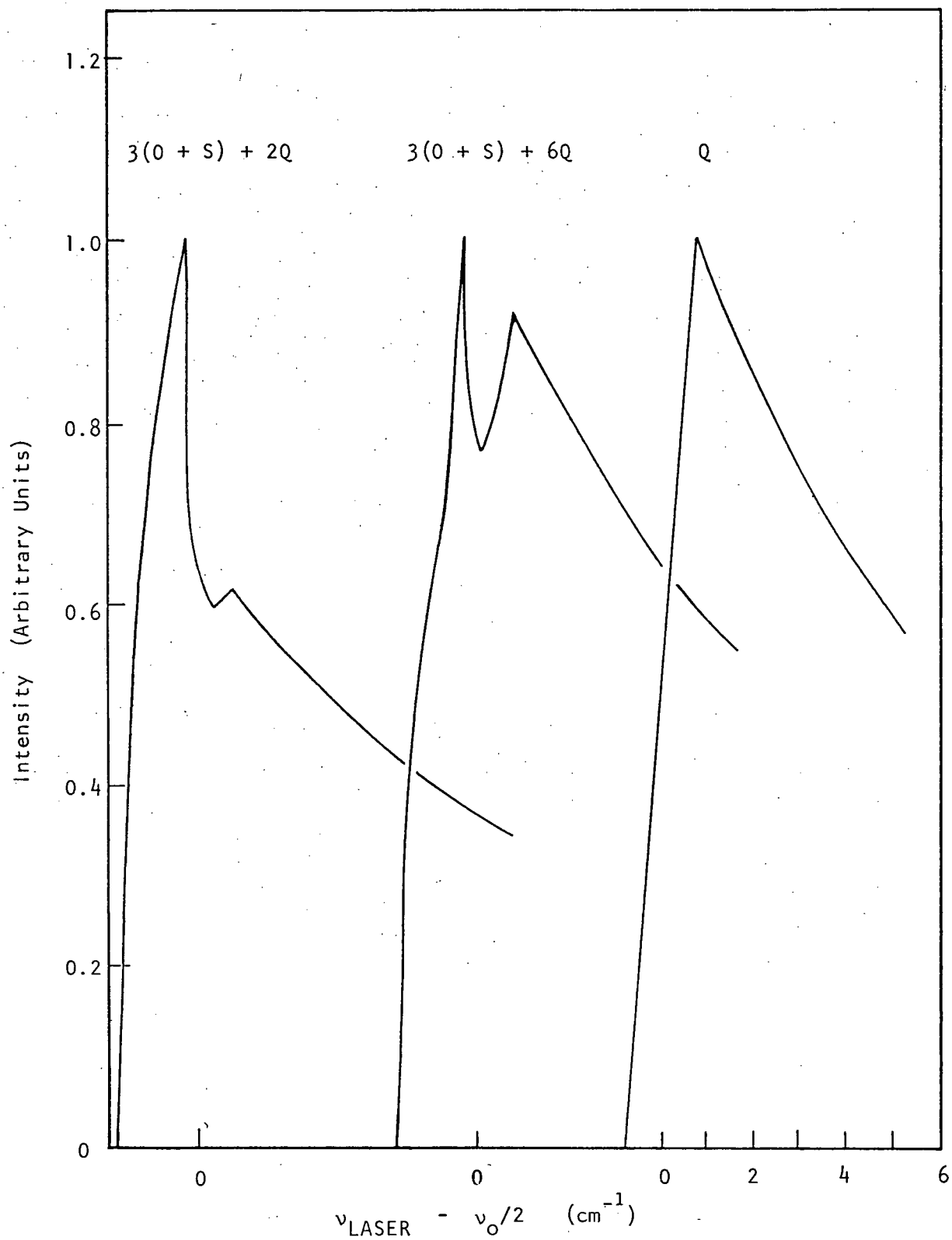
Figure 15.   Normalized Band Contour of the $0_g^+ \rightarrow 0_g^+$ Electronic Transition
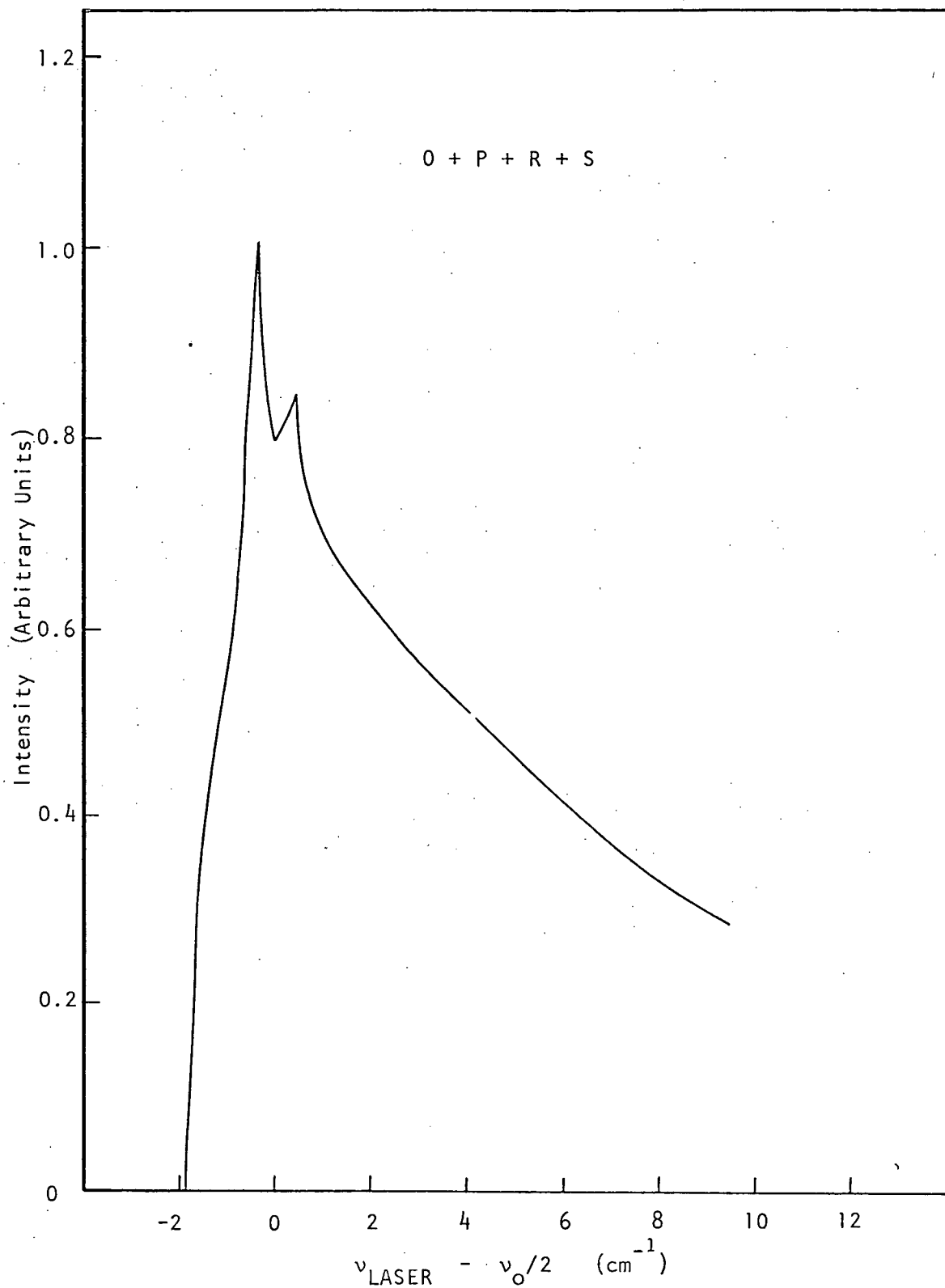
Figure 16. Normalized Band Contour of the $0_g^+ \rightarrow 1_g$ Electronic Transition
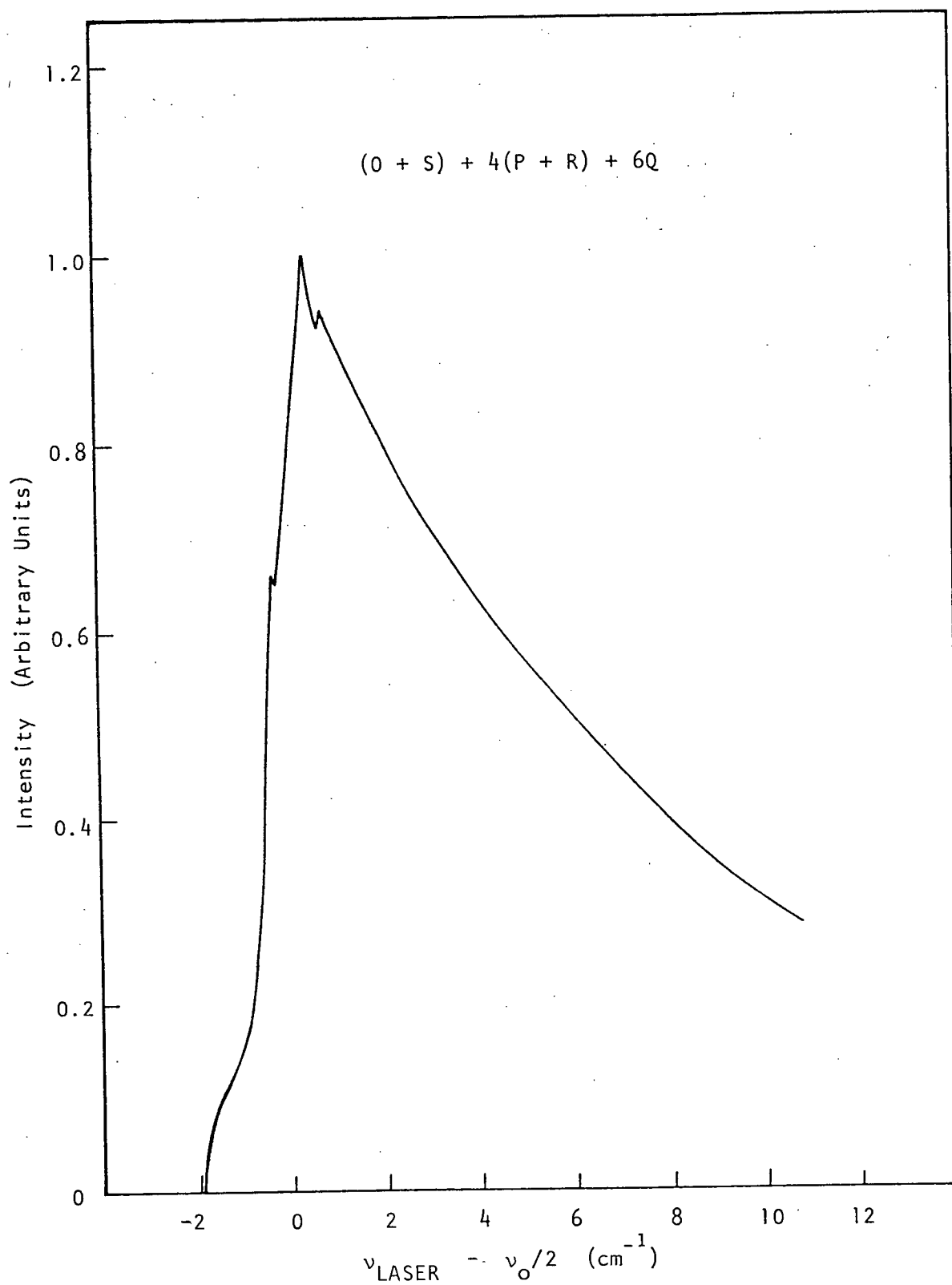
Figure 17. Normalized Band Contour of the $0_g^+ \rightarrow 2_g$ Electronic Transition

that contributions to the $0_g^+ \rightarrow 0_g^+$ transition may not be equally shared between 0_u^+ and 1_u intermediate states, as this would result in a purely Q-like band, which is not observed. Experimental investigation of the effect on the photoionization process in I_2 of polarizing the laser light (Dalby et al., 1976) firmly rules out the $0_g^+ \rightarrow 0_g^+$ electronic transition. Thus, the new electronic state observed in I_2 has, with high probability, the designation 1_g. Although the band positions were measured in the vibrational analysis from the band peak rather from the band origin ν_o, no correction was applied to T_e as this requires an exact knowledge of the bandwidth of the exciting energy.

It was noted in section 2.8 that at considerable distance from the band origin, all band configurations become Q-like with contour $I(\nu_\ell) \propto e^{-(\nu_\ell/102)(B_{v''}/\Delta B)}$ at 20^oC, where ν_ℓ is expressed in wavenumbers. Thus the ratio $\Delta B/B_{v''}$ may be estimated from the band slope at large J. For bands (4-0), (3-0), (2-0) and (0-3), $\ln[I(\nu_\ell)]$ was plotted against laser frequency ν_ℓ, each plot yielding $\Delta B/B_{v''} = 0.07$. Although this method is inherently approximate, the results compare well with the more precise Franck-Condon rotational analysis which gives $\Delta B/B_{v''} = 0.079 \pm 3\%$ (section 4.4)

4.6 Impurity Lines

Several peaks occur in the photoionization data which apparently are not members of the resonance spectrum of I_2,

being neither band-like in shape nor of the correct energy to fit the vibrational progressions. Three such peaks are clearly visible, and possibly additional peaks exist masked by the strong Iodine signal. The positions of the peaks in terms of exciting energy (in vacuum) are:

$$\nu_1 = 26{,}297.14 \pm 1 \text{ cm}^{-1}, \quad \text{Half width } 8.09 \text{ cm}^{-1}$$

$$\nu_2 = 26{,}915.22 \pm 1 \text{ cm}^{-1}$$

$$\nu_3 = 27{,}343.96 \pm 1 \text{ cm}^{-1}$$

The source of the features has not been identified. The features were developed with temperature, and remained after the Iodine vapor was cooled. Peak ν_2 is superimposed on the (1-0) band of I_2, and is very weak. Although peak ν_3 is prominent in very high voltage scans, its intensity is too low to allow accurate measurement of its power dependence. The relative intensity of the two prominent peaks is $I_{\nu_1} : I_{\nu_2} \simeq 16:1$ at 20°C. The signal at ν_1 depends upon the laser intensity to the power $I_0^{2.02}$.

5. DISCUSSION

5.1 Results and Conclusions

Quantum theory shows that the Iodine molecule must possess a rather large number of valence-shell electronic states followed, mostly at higher energies, by Rydberg states (Mulliken, 1971). For the first time, a single high-energy electronic state has been selectively populated in I_2 using the techniques of multi-photon spectroscopy. From both the requirements of energy conservation, and from experimental confirmation, the nonlinear photoelectric signal was third-order in the applied field intensity. In principle, triple-photon ionization and triple-photon dissociation were both present in the photoelectric signal. Since the dissociation yield of molecular Iodine is insignificant in comparison with the photoionization yield throughout the spectral range investigated (Myer and Samson, 1970), the predominant reaction was that of triple-photon ionization:

$$I_2 + 3\nu \rightarrow I_2^+ + e^- \ .$$
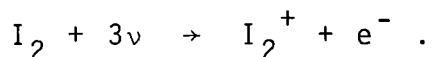
It is reasonable to assign the observed resonances to vibrational bands of two-photon transitions from the ground X 0_g^+ state to an I_2 molecular state of g symmetry. Since single-photon transitions from the ground state to such a state are parity-forbidden, this intermediate state has not previously been observed in absorption. Furthermore, the intermediate

state has no counterpart in emission spectra in the literature. The vibrational analysis was straight-forward and gave for the upper vibrational-state energies $\{T_e + G(v')\}$:

$$E(v') = 53,562.75 \pm 1 + (241.4 \pm 0.4)(v' + \tfrac{1}{2})$$
$$- (0.58 \pm 0.06)(v' + \tfrac{1}{2})^2 \text{ cm}^{-1}.$$

The rotational analysis was complex, as the bands were unresolved. Franck-Condon factors were calculated from the observed relative band intensities, and used to determine the size of the I_2 molecule in the excited state. The internuclear separation in the resonant electronic state was established at $r_e' = 2.567 \pm 0.002\overset{o}{A}$, whereupon the rotational constant is $B_e' = 0.04029 \pm 0.00007 \text{ cm}^{-1}$. These results are consistent with the observed slope of the Q-like contour of the Iodine bands at large J. The size difference of the molecule in the upper state compared to its ground state (nearly $0.1\overset{o}{A}$ smaller) indicates that the resonant electronic state is most probably a Rydberg state. Furthermore, the new state has electronic energy sufficiently high to make the category of a Rydberg state extremely probable, as a large number of Rydberg states are observed in I_2, all at energies above 51,500 cm^{-1} (Venkateswarlu, 1970).

Three electronic transitions are possible in two-photon absorption to a resonant state: $0_g^+ \rightarrow 0_g^+$, $0_g^+ \rightarrow 1_g$, and $0_g^+ \rightarrow 2_g$. Each transition has a characteristic band contour.

The theoretically predicted band contours are very similar at a resolution of 1.5 cm^{-1} and do not indicate decisively the electronic configuration of the observed resonant state in I_2. The comparison of band contours rules out only the $0_g^+ \rightarrow 2_g$ transition. Additional information was gained from polarization studies, which show that the resonant electronic state cannot have zero angular momentum. Thus it is concluded that the new electronic state has, with high probability, the designation 1_g.

The electronic potential of the new Rydberg state, approximated by a harmonic potential function, is shown in Figure 18 as a function of internuclear separation in relation to the known valence-shell states of molecular Iodine. The valence-shell potential energy diagram is reproduced from Mulliken (1971) in which the curves for states of even (g) parity are shown by full lines, and those for states of odd (u) parity by dashed lines. The potential curves of Mulliken are zeroth order approximations except for those of the ground X 0_g^+ and the B states which are rather accurately known from experimental data. The potential curve of the new Rydberg state has a minimum energy of 53,562.75 $\pm$ 1 cm^{-1} at internuclear separation 2.567 $\pm$ 0.002Å.

The photoionization efficiency $P(v',v)$ observed in Iodine has a broad functional dependence on total molecular energy (Figure 14), exhibited independently be each of our six absorption progressions. The photoionization efficiency ex-
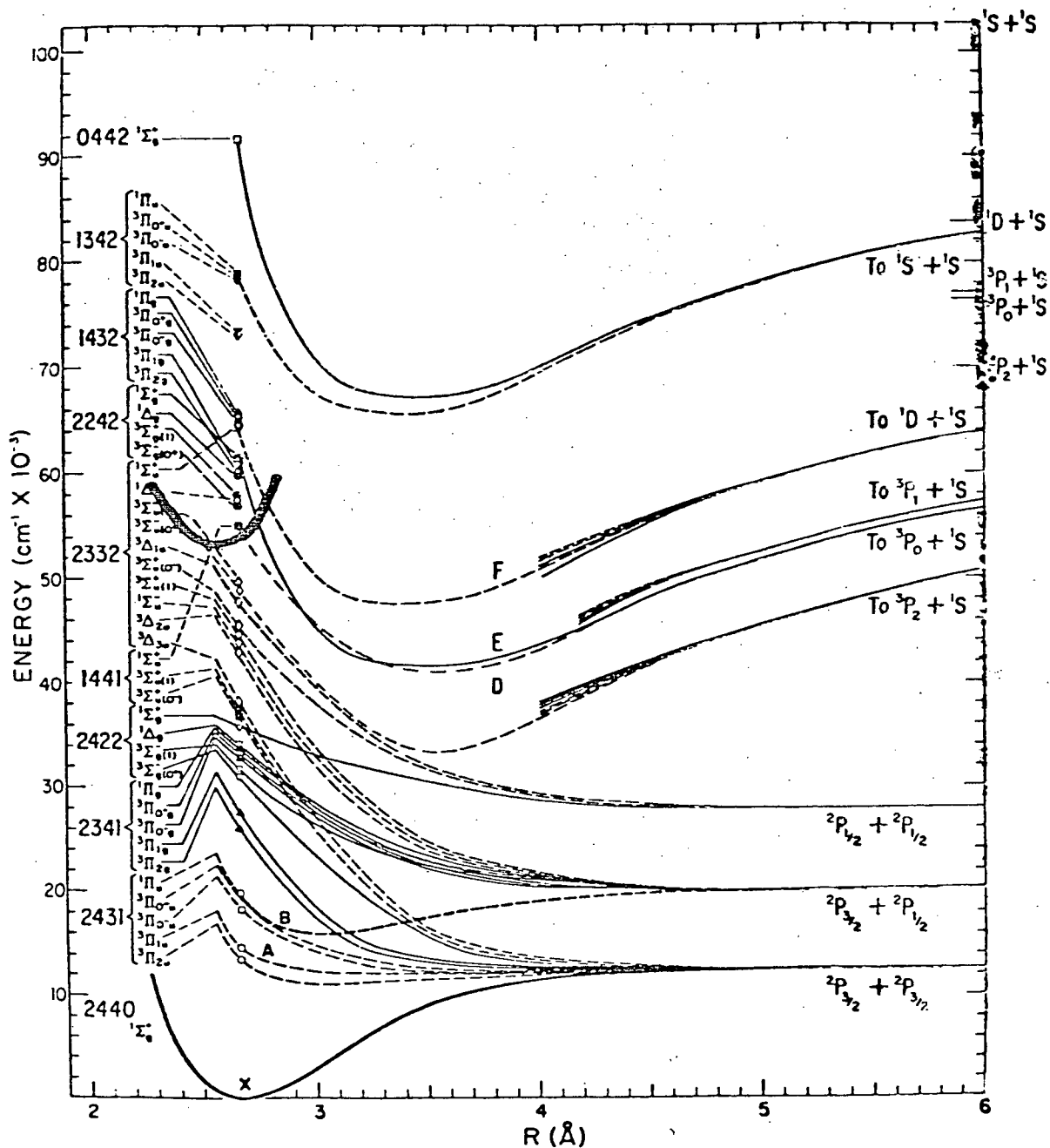
Figure 18.   Electronic Potential Diagram Including the Approximate Potential of the New State Superimposed on the Known Valence-Shell States of I_2.

hibits the slight downward trend with increasing molecular
energy observed by Myer and Samson (1970). In addition, an
apparent resonance, which is heretofore unobserved, occurs in
the vicinity of 80,000 cm^{-1} in terms of total molecular energy.
This resonant state may occur either at the level of one photon
or at the level of three photons, corresponding to electronic
energy in the vicinity of 26,700 cm^{-1} or 80,000 cm^{-1} respec-
tively. Since only the high-energy tail of the resonance was
observed, these values may be considerably lower than quoted.
The resonance in the photoionization yield $P(v',\nu)$ is
unidentifiable in the context of known electronic states of
molecular Iodine. Further investigation is required to
understand the nature of this feature appearing in the photo-
ionization yield of I_2 in nonlinear absorption.

Several spectral features were developed with temper-
ature which do not appear to be members of the resonance spec-
trum of I_2, being neither band-like in shape nor of the correct
energy to fit the vibrational progressions. One prominent im-
purity feature was observed which was second-order in the
applied field intensity, the remaining impurity features being
too weak for accurate measurement. The position of the pro-
minent peak in terms of exciting energy is 26,297.14 ± 1 cm^{-1}
with half-width 8.09 cm^{-1}. The two weaker features observed
occur at 26.915.22 ± 1 cm^{-1} and 27,343.96 ± 1 cm^{-1}. It is pos-
sible that additional peaks exist masked by the strong I_2 signal.

Identification of the source of the impurity lines is a subject for future research. If the impurity resonances also occur at the level of two photons, it is unlikely that they may be identified via atomic or molecular wavelength tables, since the transition would not exist in traditional absorption apectroscopy (the dipole-dipole transition is parity-forbidden), and since tables of emission spectra are far from complete.

5.2 Future Research

A number of subjects for future research in molecular Iodine arise directly from the present experimental work. One is the identification of the impurity lines, which most probably arise from complex molecular species formed in reactions at high temperatures with I_2. Another is the investigation of the broad functional dependence on total molecular energy of the photoionization efficiency of molecular Iodine; the resonance which appears in our data has no counterpart among the established Rydberg or valence-shell states of I_2. The nonlinear absorption of Iodine to the red of 3800Å also offers wide scope for investigation.

In a more general view, it is clear that the high-resolution techniques of laser-induced nonlinear absorption spectroscopy will yield new and significant spectroscopic information from a great number of atoms and molecules (Venkateswarlu, 1976), especially when applied to parity-forbidden and high-energy states. The effects of pertur-

bations, Stark shifts, level crossings, etc. may be in-
vestigated in atomic and molecular states heretofore in-
accessible.

APPENDIX   A

CALIBRATION OF PHOTOMULTIPLIER FILTERS

In order to avoid optical saturation of the photo-
multiplier, one or two sheets of diffusing glass plus neutral
density filter N.D.#3.0 were used to attenuate the reflected
portion of the laser beam. The materials were calibrated
with a densitometer set to give a continuous scan between
3500-4000Å. The quantity measured is called the density K,
whereby the filter's attenuation is 10^K. Since the maximum
density which may be measured is 2.0, N.D. filter #3.0,
which has a density greater than four in the ultraviolet,
could be calibrated only by placing two extra filters in the
reference beam of the densitometer. The two extra filters
(N.D.#0.9 and N.D.#1.0) had to be calibrated also (see Table
XV). The total density of the materials for the cases in which
one or two pieces of diffusing glass were used is given at
20Å intervals in Table XVI.

λ $_o$ (A)	Density of Reference Filters		Density of ND # 3.0 With #0.9 and #1.0 in Reference Beam of Densitometer (c)	Density of ND #3.0 (sum a,b,c)
	ND #0.9 (a)	ND #1.0 (b)		
3600	1.307[†]	1.670[†]	1.566[†]	4.543[††]
3620	1.287	1.648	1.537	4.472
3640	1.270	1.625	1.512	4.407
3660	1.258	1.604	1.497	4.359
3680	1.245	1.589	1.480	4.314
3700	1.232	1.573	1.468	4.273
3720	1.223	1.560	1.459	4.242
3740	1.213	1.546	1.450	4.209
3760	1.204	1.532	1.446	4.182
3780	1.194	1.520	1.411	4.155
3800	1.185	1.511	1.436	4.132
3820	1.174	1.499	1.429	4.102

[†] Uncertainty in each measurement is ± 0.002.

[††] Uncertainty in total density is ± 0.006.

Table XV.   Density of ND Filter #3.0 as a Function of Wavelength.

λ $\overset{o}{(A)}$	Density of Diffusing Glass	Density of ND Filter #3.0	Total Density Including	
			One Sheet Diffuser	Two Sheets Diffuser
3600	1.474[†]	4.543[††]	6.017[*]	7.491[**]
3620	1.474	4.472	5.946	7.420
3640	1.474	4.407	5.881	7.355
3660	1.474	4.359	5.833	7.307
3680	1.471	4.314	5.785	7.256
3700	1.469	4.273	5.742	7.211
3720	1.469	4.242	5.711	7.180
3740	1.469	4.209	5.678	7.147
3760	1.470	4.182	5.652	7.122
3780	1.471	4.155	5.626	7.097
3800	1.471	4.132	5.603	7.074
3820	1.471	4.102	5.573	7.044

[†] Uncertainty in each measurement is ± 0.001.
[††] Uncertainty is ± 0.006.
[*] Uncertainty is ± 0.007.
[**] Uncertainty is ± 0.008

Table XVI. Total Density, as a Function of Wavelength, of Materials Shielding Photomultiplier EMI 6256S.

APPENDIX   B

DETAILS OF BRANCH CONTOUR CALCULATIONS

The rotational analysis of section 4.4 allows calculation of the contours of the O, P, Q, R and S rotational branches expected in two-photon absorption. The contour $I(\nu_\ell)$ of a single branch was determined by convoluting the intensity distribution with the laser spectrum, as described in section 2.8. The parameters involved are:

$$\Delta B = 0.002951 \ cm^{-1}$$

$$B_e{}'' = 0.03735 \ cm^{-1}$$

$$B_e{}' = 0.04029 \ cm^{-1}$$

$$kT/hc = 204 \ cm^{-1} \ at \ 20^{\circ}C$$

$$Laser \ Bandwidth = 1.5 \ cm^{-1}$$

The contour of the Q-BRANCH is described completely by:

$$I_Q(\nu_\ell) = (5462)(1 - 0.911 \ e^{-(0.124)\nu_\ell}), \quad \nu_\ell \ \epsilon \ (-0.75, 0.75]$$

$$= (1018) \ e^{-(0.124)\nu_\ell}, \quad \nu_\ell \ \epsilon \ [0.75, \infty)$$

where the laser frequency ν_ℓ is expressed in wavenumbers. The contours of the O, P, R and S branches were determined from:

$$I(\nu_\ell) = 5462(e^{-J_1(J_1+1)/5462} - e^{-J_2(J_2+1)/5462})$$

with the limits of integration, J_1 and J_2, calculated at $\nu_\ell \pm 0.75 \ cm^{-1}$ from equations 2.14 to 2.17. Since the intensity distribution is an essentially continuous function

of rotational quantum number J in the spectrum of I_2, non-integral values of J are carried through the calculation. The results for each branch are:

O-BRANCH

The O-Branch forms a head at $\nu_\ell = -1.060$ cm^{-1}. The two components of the branch are described by:

(a) $J_2 = 27.31 + \sqrt{1226.8 + 677.7 \, \nu_\ell}$, $\nu_\ell \, \epsilon \, (-1.81, \infty)$

$J_1 = 27.31$, $\nu_\ell \, \epsilon \, (-1.81, -0.31]$

$= 27.31 + \sqrt{210.2 + 677.7 \, \nu_\ell}$, $\nu_\ell \, \epsilon \, (-0.31, \infty)$

(b) $J_2 = 27.31 - \sqrt{1226.8 + 677.7 \, \nu_\ell}$, $\nu_\ell \, \epsilon \, (-1.81, -0.75]$

$= 0.50$, $\nu_\ell \, \epsilon \, [-0.75, 0.75)$

$J_1 = 27.31$, $\nu_\ell \, \epsilon \, (-1.81, -0.31]$

$= 27.31 - \sqrt{210.2 + 677.7 \, \nu_\ell}$, $\nu_\ell \, \epsilon \, [-0.31, 0.75)$

P-BRANCH

The P-Branch also forms a head, at $\nu_\ell = -0.275$ cm^{-1}. The two components of the branch are described by:

(a) $J_2 = 13.65 + \sqrt{694.6 + 677.7 \, \nu_\ell}$, $\nu_\ell \, \epsilon \, (-1.025, \infty)$

$J_1 = 13.65$, $\nu_\ell \, \epsilon \, (-1.025, 0.475]$

$\doteq 13.65 + \sqrt{-322.0 + 677.7 \, \nu_\ell}$, $\nu_\ell \, \epsilon \, [0.475, \infty)$

(b) $J_2 = 13.65 - \sqrt{694.6 + 677.7 \, \nu_\ell}$, $\nu_\ell \, \epsilon \, (-1.025, 0.75]$

$\doteq 0$, $\nu_\ell \, \epsilon \, [-0.75, 0.75)$

$J_1 = 13.65$, $\nu_\ell \, \epsilon \, (-1.025, 0.475]$

$= 13.65 - \sqrt{-322.0 + 677.7 \, \nu_\ell}$, $\nu_\ell \, \epsilon \, [0.475, 0.75)$

R-BRANCH

No head is formed.

$$J_2 = -13.65 + \sqrt{667.3 + 677.7\, \nu_\ell} \quad , \quad \nu_\ell \in (-0.71, \infty)$$

$$J_1 = 0 \quad , \quad \nu_\ell \in (-0.71, 0.79]$$

$$= 13.65 + \sqrt{-349.3 + 677.7\, \nu_\ell} \quad , \quad \nu_\ell \in [0.79, \infty)$$

S-BRANCH

No head is formed.

$$J_2 = -27.31 + \sqrt{1172.2 + 677.7\, \nu_\ell} \quad , \quad \nu_\ell \in (-0.63, \infty)$$

$$J_1 = 0 \quad , \quad \nu_\ell \in (-0.63, 0.87]$$

$$= -27.31 + \sqrt{155.6 + 677.7\, \nu_\ell} \quad , \quad \nu_\ell \in [0.87, \infty)$$

REFERENCES

Bakos, J. Kiss, Á. Szabó, L. and Tendler, M.	1972	Physics Letters 39A, 283.
Baldwin, G.C.	1969	*An Introduction to Nonlinear Optics*, Plenum Press, N.Y.
Bloembergen, N.	1965	*Nonlinear Optics*, W.A. Benjamin Inc., N.Y.
Brackmann, R.T. Fite, W.L. and Hagen, K.E.	1958	Rev. Sci. Instr. 29, 125.
Cagnac, B. Grynberg, G. and Biraben, F.	1973	J. Phys. 34, 845.
Collins, C.B. Johnson, B.W. Popescu, D. Musa, G. Pascu, M.L. and Popescu, I.	1973	Physical Review 8, 2197.
Collins, C.B. Johnson, B.W. Mirza, M.Y. Popescu, D. and Popescu, I.	1974	Physical Review 10, 813.
Dalby, F.W. Petty-Sil, G. Pryce, M.H.L. and Tai, C.Y.	1976	To be published.
Dalby, F.W. and Tai, C.Y.	1976	Private communication.

Delone, G.A.
  Delone, N.B. and
  Piskova, G.K.
1972
Zh. Eksp. Teor. Fiz. 62, 1272 (Sov. Phys. - JETP 35, 672).

Finn, R.S. and
  Ward, J.F.
1971
Phys. Rev. Letters 26, 285.

Franken, P.A.
  Hill, A.E.
  Peters, C.W. and
  Weinreich, G.
1961
Phys. Rev. Letters 7, 118.

Gerry, H.T. and
  Gillespie, L.J.
1932
Physical Review 40, 269.

Giordmaine, J.A.
1962
Phys. Rev. Letters 8, 19.

Guccione-Gush, R.
  Gush, H.P. and
  Van Kranendonk, J.
1967
Can. J. Phys. 45, 2513.

Hänsch, T.W.
1972
Applied Optics 11, 895.

Haranath, P.B.V and
  Rao, P.T.
1958
J. Molec. Spectroscopy 2, 428.

Herzberg, G.
1950
Molecular Spectra and Molecular Structure, Vol. 1: Spectra of Diatomic Molecules, 2nd ed., Van Nostrand Reinhold Co., Toronto.

Hodgson, R.T.
  Sorokin, P.P. and
  Wynne, J.J.
1974
Phys. Rev. Letters 32, 343.

King, G.W.
1964
Spectroscopy and Molecular Structure, Holt, Rinehart and Winston, N.Y.

Koller, L.R.
1965
Ultraviolet Radiation, 2nd ed., John Wiley & Sons, N.Y.

Lambropoulos, P.
1974
Physical Review 9, 1992.

LeRoy, R.J.
1970a
J. Chem. Phys. 52, 2678.

LeRoy, R.J.   1970b   J. Chem. Phys. <u>52</u>, 2683.

Leung, K.M.   1974   Physical Review <u>9</u>, 2440.
   Ward, J.F. and
   Orr, B.J.

LuVan, M. and   1972a   Physics Letters <u>39A</u>, 21.
   Mainfray, G.

LuVan, M.   1972b   Phys. Rev. Letters <u>29</u>, 1134.
   Mainfray, G.
   Manus, C. and
   Tugov, I.

Mathieson, L. and   1956   J. Chem. Phys. <u>25</u>, 753.
   Rees, A.L.G.

Miles, R.B. and   1973   IEEE J. Quantum Electron.
   Harris, S.E.   <u>QE-9</u>, 470.

Millman, J. and   1972   *Integrated Electronics:*
   Halkias, C.C.   *Analog and Digital Circuits*
                                            and Systems, McGraw-Hill, N.Y.

Mulliken, R.S.   1934   Physical Review <u>46</u>, 549.

Mulliken, R.S.   1971   J. Chem. Phys. <u>55</u>, 288.

Myer, J.A. and   1970   J. Chem. Phys. <u>52</u>, 716.
   Samson, J.A.R.

Nobs, A. and   1966   Helv. Phys. Acta <u>34</u>, 564.
   Wieland, K.

Penner, S.S.   1959   *Quantitative Molecular*
                                            Spectroscopy and Gas
                                            Emissivities, Addison-
                                            Wesley Inc., Reading, Mass.

Petty, G.   1975   Phys. Rev. Letters <u>34</u>, 1207.
   Tai, C.Y. and
   Dalby, F.W.

Pindzola, M.S. and   1975   Physical Review <u>11</u>, 1543.
   Kelly, H.P.

Pryce, M.H.L.   1976   Private communciation.